Combined synchrotron-based high resolution FTIR and IR-diode laser supersonic jet spectroscopy of the chiral molecule CDBrClF

Sieghard Albert [a,*], Karen Keppler [a], Vincent Boudon [b], Philippe Lerch [c], Martin Quack [a,*]

[a] Physical Chemistry, ETH Zurich, CH-8093 Zurich, Switzerland
[b] Laboratoire Interdisciplinaire Carnot de Bourgogne, UMR 6303 CNRS-Univ. Bourgogne Franche-Comté, 9 Avenue Alain Savary, BP 47 870, F-21078 Dijon Cedex, France
[c] Swiss Light Source, Paul Scherrer Institute, CH-5232 Villigen, Switzerland

ARTICLE INFO

ABSTRACT

The rovibrational spectrum of Deuterobromochlorofluoromethane CDBrClF has been measured with a resolution of better than $0.001 \, \text{cm}^{-1}$ at room temperature with the Zurich Bruker IFS spectrometer prototype (ZP 2001) using a globar source, and with the Bruker prototype 2009 interferometer connected to the Swiss Light Source (SLS) synchrotron as a radiation source providing a resolution of $0.0007 \, \text{cm}^{-1}$ in the range $600–1100 \, \text{cm}^{-1}$. In addition CDBrClF has been measured at low rotational temperature ($T_{rot} = 15 \, \text{K}$) with our diode laser supersonic jet setup around $748 \, \text{cm}^{-1}$ in the v_5 region (resolution $0.0013 \, \text{cm}^{-1}$). The spectra of the two major isotopomers $CD^{79}Br^{35}ClF$ and $CD^{81}Br^{35}ClF$ have been analyzed within the v_5 (CCl-stretch, $\tilde{v}_0 = 748.2998 \, \text{cm}^{-1}$ ($CD^{79}Br^{35}ClF$), $\tilde{v}_0 = 748.1541 \, \text{cm}^{-1}$ ($CD^{81}Br^{35}ClF$)), v_4 (CF-stretch, $\tilde{v}_0 = 1082.8116 \, \text{cm}^{-1}$ ($CD^{79}Br^{35}ClF$), $\tilde{v}_0 = 1082.7963 \, \text{cm}^{-1}$ ($CD^{81}Br^{35}ClF$)) and v_3 (DCF-bend, $\tilde{v}_0 = 918.3715 \, \text{cm}^{-1}$ ($CD^{79}Br^{35}ClF$), $\tilde{v}_0 = 918.0206 \, \text{cm}^{-1}$ ($CD^{81}Br^{35}ClF$)) regions. A detailed rovibrational analysis of these bands is presented. A combined analysis of the v_3, v_4 and v_5 fundamental bands provides accurate rotational and quartic centrifugal distortion constants for the vibrational ground state and for the states v_3, v_4 and v_5 of $CD^{79}Br^{35}ClF$ and $CD^{81}Br^{35}ClF$. The results are discussed in relation to intramolecular (ro)vibrational redistribution (IVR) and also possible experiments pertaining to the experimental detection of molecular parity violation.

1. Introduction

The high resolution microwave spectroscopy of chiral molecules has a considerable history with results including quite complex molecules such as amino acids, biphenyls or chiral complexes ([1–8] and references cited therein). The high resolution infrared spectroscopy of chiral molecules has started much later, beginning in the mid 1990s (see [9–16] and references cited therein). In particular, recent interest in the high resolution IR-spectroscopy of chiral molecules has arisen from the possibility of experimental studies of molecular parity violation (see [15–19]). In this context as in the context of intramolecular energy flow the prototypical chiral molecule CHBrClF has been studied experimentally and theoretically in some detail [9,10,20–28]. As a prototype for molecular structure CHBrClF has been of historical interest [29,30] and its synthesis has been reported early on (see [31] and references

therein). The structure has been derived from microwave spectra [10] including the Urey–Bradly force field from low resolution vibrational spectra [32–34]. Studies of vibrational circular dichroism (VCD) and Raman optical activity (ROA) have finally led to a determination of absolute molecular configuration [35–37] mentioning also the possible application of the Coulomb explosion technique with this molecule [38–43]. This summary of work on CHBrClF is by no means exhaustive. The isotopomer CDBrClF (Fig. 1) has been studied much less, initially together with CHBrClF [32–36]. A broad coverage of vibrational spectra in the infrared and near infrared has led to information about intramolecular vibrational redistribution including multidimensional wavepackets [44]. The influence of the strong anharmonic coupling on the parity violating energy difference between the enantiomers of CDBrClF has been investigated in [28] (see also [45]). We have reported some preliminary results on high resolution infrared spectra in [12–14,16].

The aim of the present investigation is a detailed high resolution spectroscopic analysis of the infrared spectra in the range of the fundamentals v_3, v_4 and v_5 covering the range $600–1200 \, \text{cm}^{-1}$. With this goal in mind we have combined our experi-

* Corresponding authors at: Physical Chemistry, ETH Zurich, CH-8093 Zurich, Switzerland.

E-mail addresses: albert@ir.phys.chem.ethz.ch (S. Albert), martin@quack.ch (M. Quack).
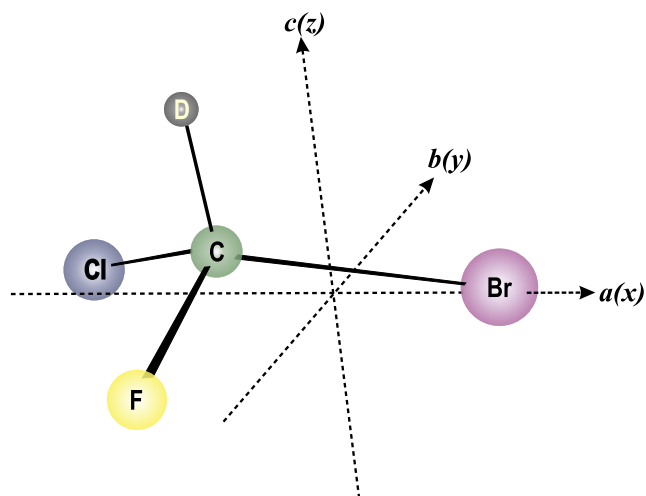
Fig. 1. Equilibrium structure and principal axes a, b, c of CDBrClF and Cartesian axes definitions.

mental results from three different techniques: high resolution Fourier transform infrared (FTIR) with a thermal (globar) light source, achieving an instrumental resolution of about 0.001 cm^{-1} or better [14], FTIR spectroscopy with a synchrotron light source (achieving an unapodized instrumental resolution of 0.0005 cm^{-1} at best) [46–50] and diode laser infrared spectroscopy of CDBrClF in a seeded supersonic jet expansion, achieving an effective rotational temperature of about 15 K [51]. Section 2 reports some experimental details, Section 3 discusses the assignment proce-

dures and results and Section 4 reports the detailed results of the rovibrational analysis. We conclude in Section 5 with a discussion of the results in the context of intramolecular vibrational redistribution (IVR) and of possible spectroscopic studies of molecular parity violation. Fig. 2 shows a graphical survey of the normal vibrations of CDBrClF.

2. Experimental

The infrared spectrum of CDBrClF recorded at room and at low temperatures has been measured with three different setups; at room temperature with the Zurich Bruker IFS prototype spectrometer ZP 2001 including a globar source in the range 600–2200 cm^{-1} (resolution better than 0.001 cm^{-1}) and with the Bruker interferometer prototype 2009 connected to the Swiss Light Source (SLS)-synchrotron located at the Paul Scherrer Institute. Here, a resolution of 0.0007 cm^{-1} was possible in the range 600–900 cm^{-1}. Fig. 3 shows a survey of the high resolution FTIR spectrum of CDBrClF in the range 600–1300 cm^{-1}. CDBrClF was also measured at low temperature with our diode laser jet setup around 748 cm^{-1} in the ν_5 region. The spectrum of the two major isotopomers has been analyzed within the ν_5 (CCl-stretch), ν_4 (CF-stretch) and ν_3 (DCF-bend) regions and a detailed rovibrational analysis of these bands is presented. CDBrClF has been synthesized by a modification of the decarboxylation of deuterobromochloro fluoroacetic acid according to Doyle and Vogl [31]. A more detailed description is given in Ref. [44]. The characterization of the sample was obvious from the high resolution spectra, which also indicated the presence of CHBrClF as minor impurity.
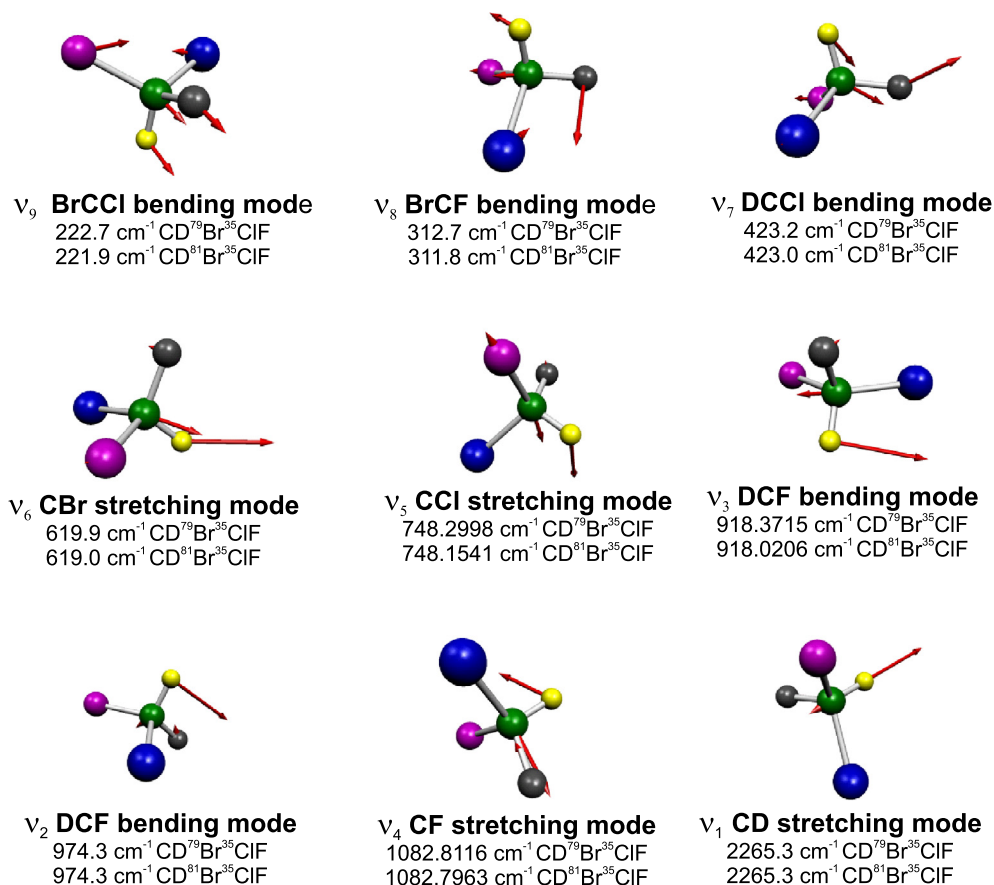

ν_9 **BrCCl bending mode**
222.7 cm^{-1} CD^{79}Br^{35}ClF
221.9 cm^{-1} CD^{81}Br^{35}ClF

ν_8 **BrCF bending mode**
312.7 cm^{-1} CD^{79}Br^{35}ClF
311.8 cm^{-1} CD^{81}Br^{35}ClF

ν_7 **DCCl bending mode**
423.2 cm^{-1} CD^{79}Br^{35}ClF
423.0 cm^{-1} CD^{81}Br^{35}ClF

ν_6 **CBr stretching mode**
619.9 cm^{-1} CD^{79}Br^{35}ClF
619.0 cm^{-1} CD^{81}Br^{35}ClF

ν_5 **CCl stretching mode**
748.2998 cm^{-1} CD^{79}Br^{35}ClF
748.1541 cm^{-1} CD^{81}Br^{35}ClF

ν_3 **DCF bending mode**
918.3715 cm^{-1} CD^{79}Br^{35}ClF
918.0206 cm^{-1} CD^{81}Br^{35}ClF

ν_2 **DCF bending mode**
974.3 cm^{-1} CD^{79}Br^{35}ClF
974.3 cm^{-1} CD^{81}Br^{35}ClF

ν_4 **CF stretching mode**
1082.8116 cm^{-1} CD^{79}Br^{35}ClF
1082.7963 cm^{-1} CD^{81}Br^{35}ClF

ν_1 **CD stretching mode**
2265.3 cm^{-1} CD^{79}Br^{35}ClF
2265.3 cm^{-1} CD^{81}Br^{35}ClF

Fig. 2. The nine normal modes of CDBrClF. The amplitudes of the harmonic normal vibrations are indicated by the arrows, the wavenumbers correspond to the fundamentals from experiment.
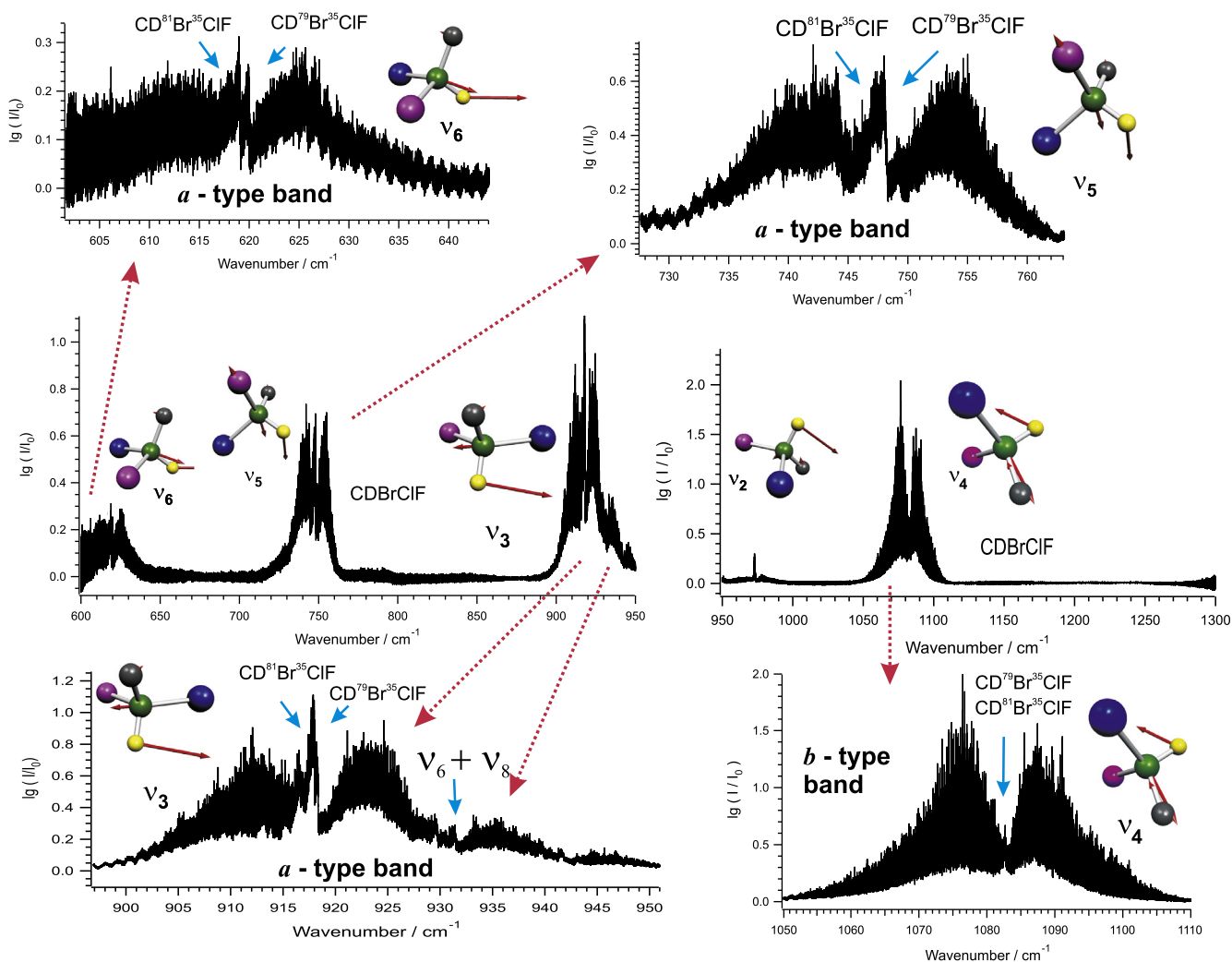
Fig. 3. Overview spectrum of CDBrClF between 600 and 1300 cm^{-1} with the ν_6, ν_5, ν_3, $\nu_6 + \nu_8$, ν_2 and ν_4 bands.

2.1. Synchrotron-based and globar-based FTIR spectra

The ETH-SLS Bruker IFS 125 HR prototype 2009 [46–50] with the currently worldwide highest available Maximum Optical Path Difference of $d_{MOPD} = 11.7$ m, including transfer optics interfacing it to the infrared port available at the Swiss Light Source (SLS) is shown in Fig. 4. Synchrotron radiation extracted out of the storage ring is steered along three segments of 1:1 optics using Al coated mirrors kept under vacuum. From the third focal point, the beam is further steered through dedicated transfer optics to the FTIR spectrometer. The transfer optics shown in Fig. 4 consist of one parabolic, two toroidal and one flat mirror. The toroidal mirrors are necessary due to the strong astigmatism of the synchrotron radiation. A parallel beam entering the source chamber of the spectrometer is focused through a parabolic mirror with focal length 41.8 cm to the aperture, which might have a diameter as small as 0.5 mm, and passes on into the interferometer. The interferometer has an unapodized resolution of 0.00052 cm^{-1} or 16 MHz. The spectrometer is a further development of our IFS 120/125 prototype 2001 [12–14] which has a $d_{MOPD} = 9.8$ m and an unapodized resolution of 0.0007 cm^{-1}, which was also used in the present work.

The FTIR spectrum of CDBrClF was recorded using synchrotron radiation at 295 K in the region 600–900 cm^{-1} with an aperture of 0.8 mm and a $d_{MOPD} = 11.7$ m. Due to self-apodization the effective instrumental resolution is around 0.0007 cm^{-1}, slightly larger than the unapodized resolution, but slightly smaller than the Doppler width (0.0009 cm^{-1} at 800 cm^{-1}) for this molecule in this spectral region. Sample pressures of 0.05 to 0.2 mbar for CDBrClF were used to exclude pressure broadening, expected to be less than 0.0001 cm^{-1} under these conditions. The room temperature spectra were recorded in a White-type cell with path lengths up to 19.2 m. 80 scans were co-added.

In addition, the IR spectrum of CDBrClF was measured in the range between 600 and 1300 cm^{-1} with the Zurich Bruker FTIR spectrometer ZP 2001 at room temperature using a globar source and an aperture of 1 mm leading to an effective resolution of 0.001 cm^{-1} or better. A White-type cell with a path length ranging from 3.2 m up to 19.2 m was also used for the CDBrClF measurements. The sample pressure was varied from 0.09 to 1.3 mbar. All spectra were self-apodized. Table 1 summarizes the measurement parameters. The wavenumbers were calibrated with OCS as standard [52].

2.2. Diode laser jet spectra

The diode laser spectra have been recorded with an instrumental resolution of 0.0013 cm^{-1} using a pulsed slit jet apparatus which has been described previously [9,10,53,54,51]. A lead salt diode laser emitting in this wavenumber range was obtained from Laser Analytics. In order to improve the vibrational cooling CDBrClF has been mixed with helium with a CDBrClF:He seeding
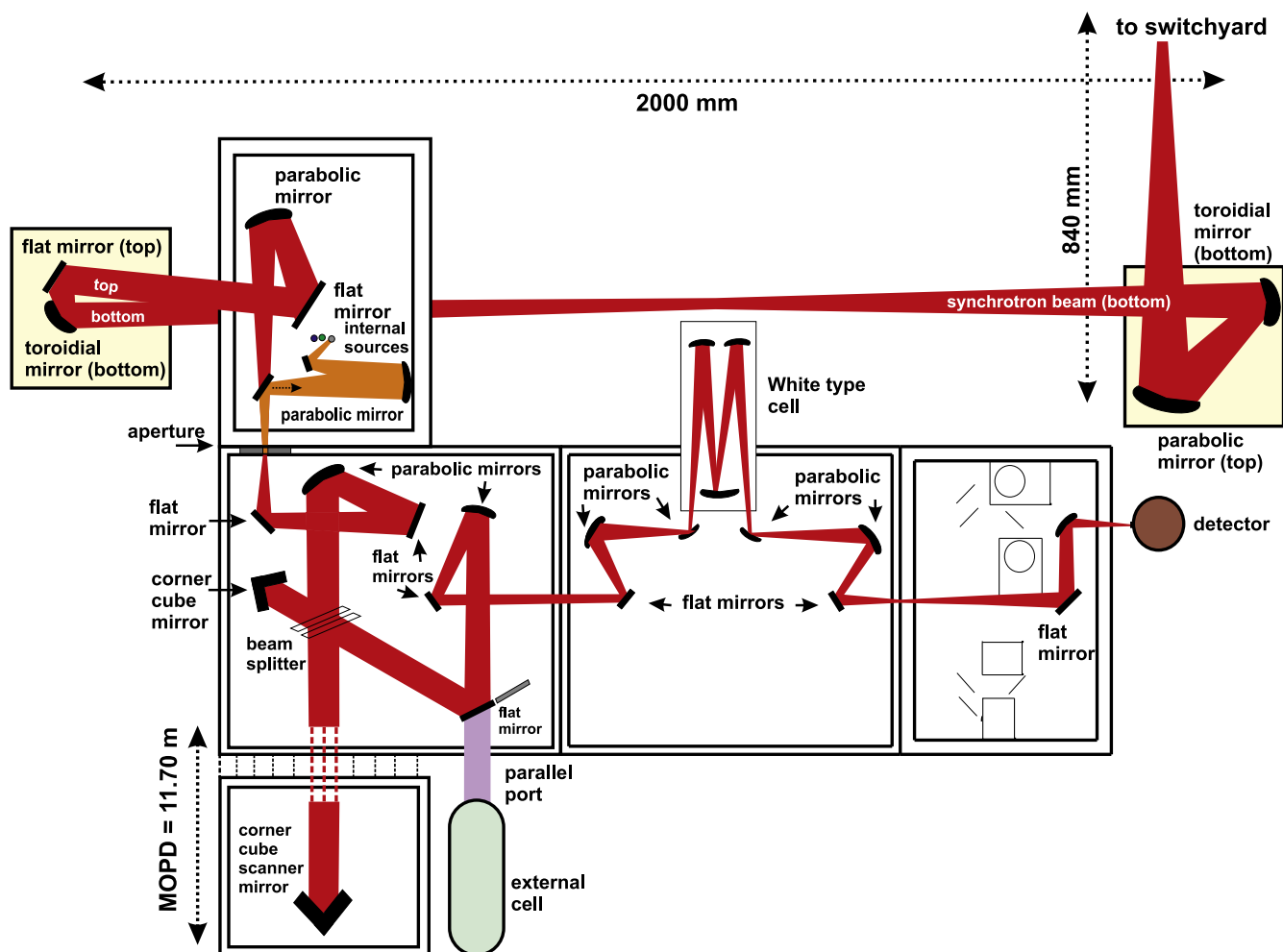
Fig. 4. Setup of the ETH-SLS Bruker IFS 125 prototype 2009 at the Swiss Light Source (SLS). The synchrotron radiation coming from the switchyard is guided through transfer optics consisting of four mirrors into the source chamber of the interferometer where it is focused and passed through an aperture into the interferometer chamber.

Table 1
Measurement parameters for the region 600–1300 cm^{-1} of the infrared spectrum of CDBrClF.

Region (cm^{-1})	Resolution (cm^{-1})	Windows	Source	Detector	Beamsplitter	Opt. filter (cm^{-1})	Aperture (mm)	ν_{mirror} (kHz)	Electr. filter (cm^{-1})	Calib. gas
600–1000	0.001	KBr	Globar	MCT	Ge:KBr	550–1000	1.0	40	395–1580	OCS [52]
600–900	0.0008	KBr	Synchrotron	MCT	Ge:KBr	550–900	0.8	40	395–1580	OCS [52]
950–1300	0.001	KBr	Globar	MCT	Ge:KBr	550–1000	1.0	40	395–1780	OCS [52]

ratio of 1:4 which has led to rotational temperatures in the range $T_{rot} = 15$–40 K. The sample mixture was pulsed through a 0.5×35 mm slit nozzle with a frequency below 0.5 Hz and an opening time of 2.5 ms. The backing pressure was 350 mbar. Multi-reflection optics consisting of two flat mirrors mounted on both sides of the slit allowing up to nine passes have been used to improve the sensitivity of the scan. Two spectral regions 747.9–748.4 cm^{-1} ($J = 1$–12) and 748.9–749.8 cm^{-1} ($J = 5$–11) have been scanned with the single-mode diode. CDCl$_3$ was used as reference gas to calibrate the laser spectra. The CDCl$_3$ lines themselves have been calibrated against NH$_3$ lines measured with an FTIR spectrometer with an accuracy of 0.0005 cm^{-1}.

3. Assignment

CDBrClF exists as a mixture of four isotopomers (due to the ^{35}Cl/^{37}Cl and ^{79}Br/^{81}Br ratios) with an abundance of 0.380

(CD^{79}Br^{35}ClF): 0.369 (CD^{81}Br^{35}ClF): 0.122 (CD^{79}Br^{37}ClF): 0.118 (CD^{81}Br^{37}ClF). Due to the two heavy atoms and their isotopes the rotational structure of the bands is dense and congested. In addition, due to the C$_1$ symmetry, only hybrid bands have been seen in the spectrum. In the present work the ν_3 (DCF-bend) ν_4 (CF-stretch) and ν_5 (CCl-stretch) bands of the two major isotopomers CD^{79}Br^{35}ClF and CD^{81}Br^{35}ClF have been analyzed. The spectral features of the minor isotopomers from ^{37}Cl are visible in the spectrum. However, a straightforward analysis was not possible at this time. In the following description the term 'subband' or 'series' describes the transitions belonging to one K_a or K_c value. The assignment of the observed rovibrational transitions belonging to a particular subband characterized by K_a and K_c series and consisting of P and R branches has been carried out efficiently with an interactive Loomis-Wood (LW) assignment program originally designed for linear molecules [55–62] (see also [63]). This graphical pattern recognition and assignment program is a very powerful
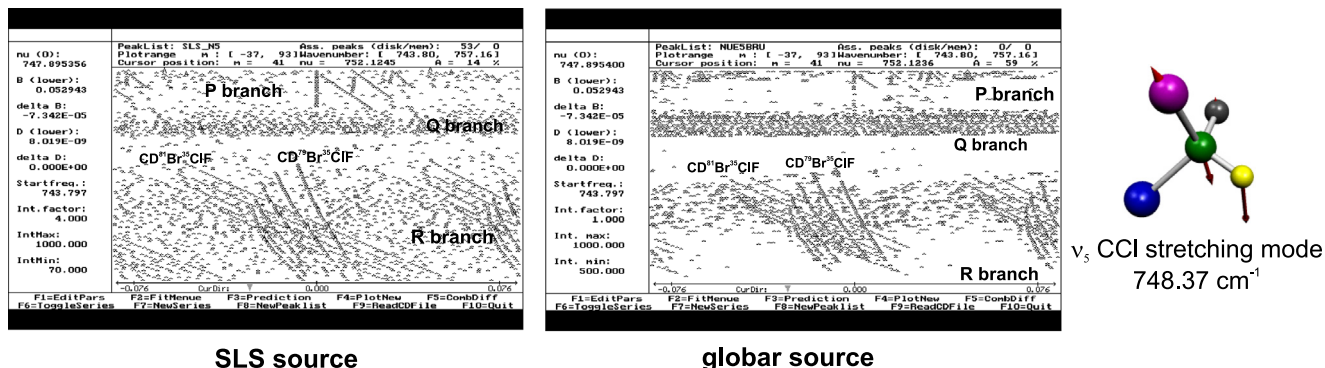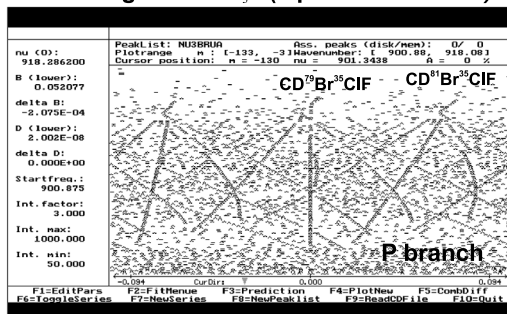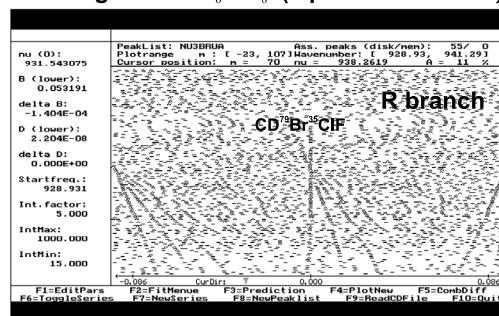
Loomis-Wood diagrams of ν_5 (J plotted versus C)

SLS source   globar source

ν_5 CCl stretching mode
748.37 cm^{-1}

LW diagrams of ν_3 (J plotted versus C)   LW diagrams of $\nu_6 + \nu_8$ (J plotted versus C)

ν_3 DCF bending mode
917.86 cm^{-1}

ν_8 BrCF bending mode ν_6 CBr stretching mode

$\nu_6 + \nu_8$

Fig. 5. Upper part: Loomis-Wood diagram of the ν_5 band of CDBrClF recorded with the SLS as source (left) and the globar as source (right). P- and R-branches of the a-type series are shown. The improved signal-to-noise ratio of the SLS spectrum compared to the globar spectrum is visible. The rotational quantum number J is plotted versus the rotational constant C. The vertical series belong to the isotopomer CD^{79}Br^{35}ClF and the slanted series belong to the isotopomer CD^{81}Br^{35}ClF. Lower part: Loomis-Wood diagram of the ν_3 band of CDBrClF (left). The rotational quantum number J is plotted versus the rotational constant C. P-branches of the a-type series are shown. The series of the two major isotopomers CD^{79}Br^{35}ClF and CD^{81}Br^{35}ClF are visible. Loomis-Wood plot of the $\nu_6 + \nu_8$ band of CDBrClF (right). R-branches of the a-type series are shown.

tool and allows also the assignment of absorption patterns of oblate [64] and prolate [65–68] asymmetric top molecules.

3.1. Assignment of the ν_5 fundamental (CCl-stretch) of CD^{79}Br^{35}ClF and (CD^{81}Br^{35}ClF)

The CCl-stretching spectral region of CDBrClF was measured using three different techniques: (i) the high resolution ($\Delta\tilde{\nu} = 0.001$ cm^{-1}, full width at half maximum, FWHM) Zurich Bruker FTIR prototype spectrometer ZP2001 using a thermal radiation source (globar), (ii) the ETH-SLS Bruker FTIR prototype spectrometer 2009 using synchrotron radiation ($\Delta\tilde{\nu} = 0.0008$ cm^{-1}, FWHM) and (iii) a diode laser jet setup providing spectra at low rotational temperatures below 20 K with an effective resolution of $\Delta\tilde{\nu} = 0.0013$ cm^{-1} (FWHM). The ν_5 fundamental of CD^{79}Br^{35}ClF and CD^{81}Br^{35}ClF consists mainly of a-type transitions defined as $(J \pm 1, K_a, K_c = J \pm 1 - K_a) \leftarrow (J, K_a, K_c = J - K_a)$ and shows clearly the characteristic overall shape of an a-type band (Fig. 3). The b- and c-type transitions of the ν_5 fundamental are not detectable. The a-type transitions of CD^{79}Br^{35}ClF and CD^{81}Br^{35}ClF have been assigned using a Loomis-Wood assignment program. As the Loomis-Wood digrams in Fig. 5 (upper part) illustrate, showing the R branch and part of the P branch, the assignment is relatively

easy if the lines are resolved. The different K_a series are clearly visible. Absorption lines up to $J \leqslant 100, K_a \leq 10$ and $K_c = J - K_a$ have been assigned for CD^{79}Br^{35}ClF and CD^{81}Br^{35}ClF. Another advantage of the Loomis-Wood diagrams is also displayed: one can easily distinguish between the two major isotopomers CD^{79}Br^{35}ClF and CD^{81}Br^{35}ClF (see descriptions in the figure and caption to Fig. 5).

A comparison of the globar and SLS spectrum of the ν_5 band of CDBrClF displayed in Fig. 7 (upper part) and in the enlarged parts in Fig. 8 illustrates the much better signal-to-noise ratio of the SLS spectrum compared to the globar spectrum. Due to the lower noise a combination band of CD^{79}Br^{35}ClF and CD^{81}Br^{35}ClF assigned as $\nu_7 + \nu_8$ has been identified in the SLS spectrum. In addition, the ν_5 band of CHBrClF present as an impurity is also visible in the SLS spectrum. This impurity is not detectable in the globar spectrum due to the larger noise level, as a comparison of the top and second traces in the upper part of Fig. 7 illustrates.

The jet-cooled diode laser spectra (Fig. 9) have been used to resolve and assign the Q branch regions of CD^{79}Br^{35}ClF and CD^{81}Br^{35}ClF around 748 cm^{-1}. Due to the low temperature of 15 K it was possible to assign absorption lines from $J = 2$ up to $J = 12$. In addition, a-type R-branch lines around 749 cm^{-1} (Fig. 10) have been assigned for CD^{79}Br^{35}ClF and CD^{81}Br^{35}ClF in the range $J = 5$–11. Due to the assignment of lower J values it

Loomis-Wood diagram of *J* plot versus *C*

```
nu (O):
1080.305156    PeakList: WC_N4NC         Ass. peaks (disk/mem):  74/  0
               Plotrange   m: [ -101,  29]Wavenumber: [ 1069.16, 1083.50]
B (lower):     Cursor position:  m =  29  nu =  1083.4952      A =   1 %
   0.053501
                           CD⁸¹Br³⁵ClF
delta B:
  -2.293E-05
D (lower):
   0.000E+00
delta D:
   0.000E+00
Startfreq.:
   1069.159
Int.factor:
   1.000                                         CD⁷⁹Br³⁵ClF
IntMax:
   1000.000
IntMin:
   120.000                         P branch
               -0.096        CurDir:      0.000              0.096
               F1=EditPars   F2=FitMenue  F3=Prediction  F4=PlotNew  F5=CombDiff
               F6=ToggleSeries F7=NewSeries F8=NewPeakList F9=ReadCDFile F10=Quit
```

Loomis-Wood diagram of *J* plot versus (*B+C*)/2

```
nu (O):
1082.234780    PeakList: WC_N4NC         Ass. peaks (disk/mem):  77/  0
               Plotrange   m: [ -259,-129]Wavenumber: [ 1050.67, 1066.62]
B (lower):     Cursor position:  m = -129  nu =  1066.6198      A =   4 %
   0.060800
                 CD⁸¹Br³⁵ClF              P branch
delta B:
  0.000E+00
D (lower):
  0.000E+00                          CD⁷⁹Br³⁵ClF
delta D:
  0.000E+00
Startfreq.:
   1050.667
Int.factor:
   1.000
IntMax:
   1000.000
IntMin:
   0.000
               -0.066        CurDir:      0.000              0.066
               F1=EditPars   F2=FitMenue  F3=Prediction  F4=PlotNew  F5=CombDiff
               F6=ToggleSeries F7=NewSeries F8=NewPeakList F9=ReadCDFile F10=Quit
```

```
nu (O):
1082.234780    PeakList: WC_N4NC         Ass. peaks (disk/mem):  77/  0
               Plotrange   m: [ -67,  63]Wavenumber: [ 1051.21, 1105.45]
B (lower):     Cursor position:  m = -5  nu =  1080.0520      A =   5 %
   0.208509
                          P branch  CD⁸¹Br³⁵ClF
delta B:                                    CD⁷⁹Br³⁵ClF
  -7.314E-04
D (lower):
   2.321E-07
delta D:
   0.000E+00
Startfreq.:
   1051.215
Int.factor:
   1.000
IntMax:
   1000.000
IntMin:
   50.000                        R branch
               -0.113        CurDir:      0.000              0.113
               F1=EditPars   F2=FitMenue  F3=Prediction  F4=PlotNew  F5=CombDiff
               F6=ToggleSeries F7=NewSeries F8=NewPeakList F9=ReadCDFile F10=Quit
```

ν_4 CF stretching mode
1080.67 cm⁻¹

Loomis-Wood diagram of *J* plot versus *A*

Fig. 6. Loomis-Wood plot of the ν_4 band of CDBrClF recorded with the globar as source. P-branches of the *b*-type (*a*-type) series are shown (top, left). The rotational quantum number *J* is plotted versus the rotational constant *C*. The vertical series belong to the isotopomer CD⁷⁹Br³⁵ClF and the slanted series belong to the isotopomer CD⁸¹Br³⁵ClF. Top, right: Loomis-Wood plot of the ν_4 band of CDBrClF. P-branches of the *b*-type series are shown. The rotational quantum number *J* is plotted versus the rotational constants $(B + C)/2$. The two major isotopomers CD⁷⁹Br³⁵ClF and CD⁸¹Br³⁵ClF are easily distinguishable. Bottom left: Loomis-Wood plot of the ν_4 band of CDBrClF. P-branches of the *b*-type (*c*-type) series are shown. The rotational quantum number *J* is plotted versus the rotational constant *A*.

was possible to detect the asymmetry splitting of the R-branch lines.

3.2. Assignment of the ν_3 fundamental (DCF-bending) of CD⁷⁹Br³⁵ClF and CD⁸¹Br³⁵ClF

The DCF-bending fundamental region of CDBrClF was measured at room temperature with the high resolution ($\Delta \tilde{v} = 0.001$ cm⁻¹) Zurich Bruker FTIR spectrometer ZP2001 using thermal source radiation (globar). The ν_3 fundamental of CD⁷⁹Br³⁵ClF and CD⁸¹Br³⁵ClF consists mainly of *a*-type transitions and shows the band shape of an *a*-type band, as one can see in Figs. 3, 12 and 13. In addition, a combination *a*-type band $\nu_6 + \nu_8$ of the two major isotopomers CD⁷⁹Br³⁵ClF and CD⁸¹Br³⁵ClF has also been identified in this region. According to the Loomis-Wood diagrams in Fig. 5 (lower part, left and right) the combination band and the ν_3 fundamental of CD⁷⁹Br³⁵ClF and CD⁸¹Br³⁵ClF show similar K_a series patterns. All K_a transition series of each band and isotopomer overlap within a few *J* values. Absorption lines up to $J \leqslant 110, K_a \leq 12$ and $K_c = J - K_a$ of the ν_3 fundamental have been assigned for CD⁷⁹Br³⁵ClF and CD⁸¹Br³⁵ClF using Loomis-Wood diagrams. The identification of the different K_a series was more difficult compared to the ν_5 assignment procedure and has only been carried out using combination differences. A more detailed observation identifies local resonances between $J = 70$ and $J = 85$ for CD⁷⁹Br³⁵ClF and between $J = 65$ and $J = 80$ for CD⁸¹Br³⁵ClF of each assigned K_a series. The $\nu_6 + \nu_8$ state acts as the resonance partner. The Loomis-Wood diagram of the $\nu_6 + \nu_8$ combination band (Fig. 5,

lower part, right) illustrates local perturbations. An assignment of the $\nu_6 + \nu_8$ band was carried out in the R branch region of the band.

3.3. Assignment of the ν_4 fundamental (CF-stretch) of CD⁷⁹Br³⁵ClF and CD⁸¹Br³⁵ClF

The CF-stretching fundamental region of CDBrClF was also measured at room temperature with the high resolution ($\Delta \tilde{v} = 0.001$ cm⁻¹) Zurich Bruker FTIR spectrometer ZP2001 using a globar. The ν_4 fundamental of CDBrClF has a *b*-type band shape as shown in Fig. 3. The very weak Q branch is barely visible. Despite the congested spectrum at room temperature it was not necessary to decrease the rotational temperature of the sample in order to simplify the spectra, because the different series of transitions were clearly visible in the spectra. Due to the low symmetry of the molecule the *b*-type transitions with $(J \pm 1, K_a \pm 1, K_c = J \pm 1 - K_a) \leftarrow (J, K_a, K_c = J - K_a)$ coincide with *a*-type transitions with $(J \pm 1, K_a, K_c = J \pm 1 - K_a) \leftarrow (J, K_a, K_c = J - K_a)$ and the *b*-type transitions with $(J \pm 1, K_a = J \pm 1 - K_c, K_c \pm 1) \leftarrow (J, K_a = J - K_c, K_c)$ coincide with *c*-type transitions $(J \pm 1, K_a = J \pm 1 - K_c, K_c) \leftarrow (J, K_a = J - K_c, K_c)$. This fact is nicely illustrated in the Loomis-Wood diagrams shown in Fig. 6. The Loomis-Wood diagram shown on the top left plots the transitions versus the rotational *C* constant; the different K_a series up to 6 are visible. This is the region where the *b*-type transitions coincide with *c*-type transitions. As one can see, the two major isotopomers CD⁷⁹Br³⁵ClF and CD⁸¹Br³⁵ClF can easily be distinguished and assigned. In the other Loomis-Wood diagram (top right) the transitions are plotted versus $(B + C)/2$.
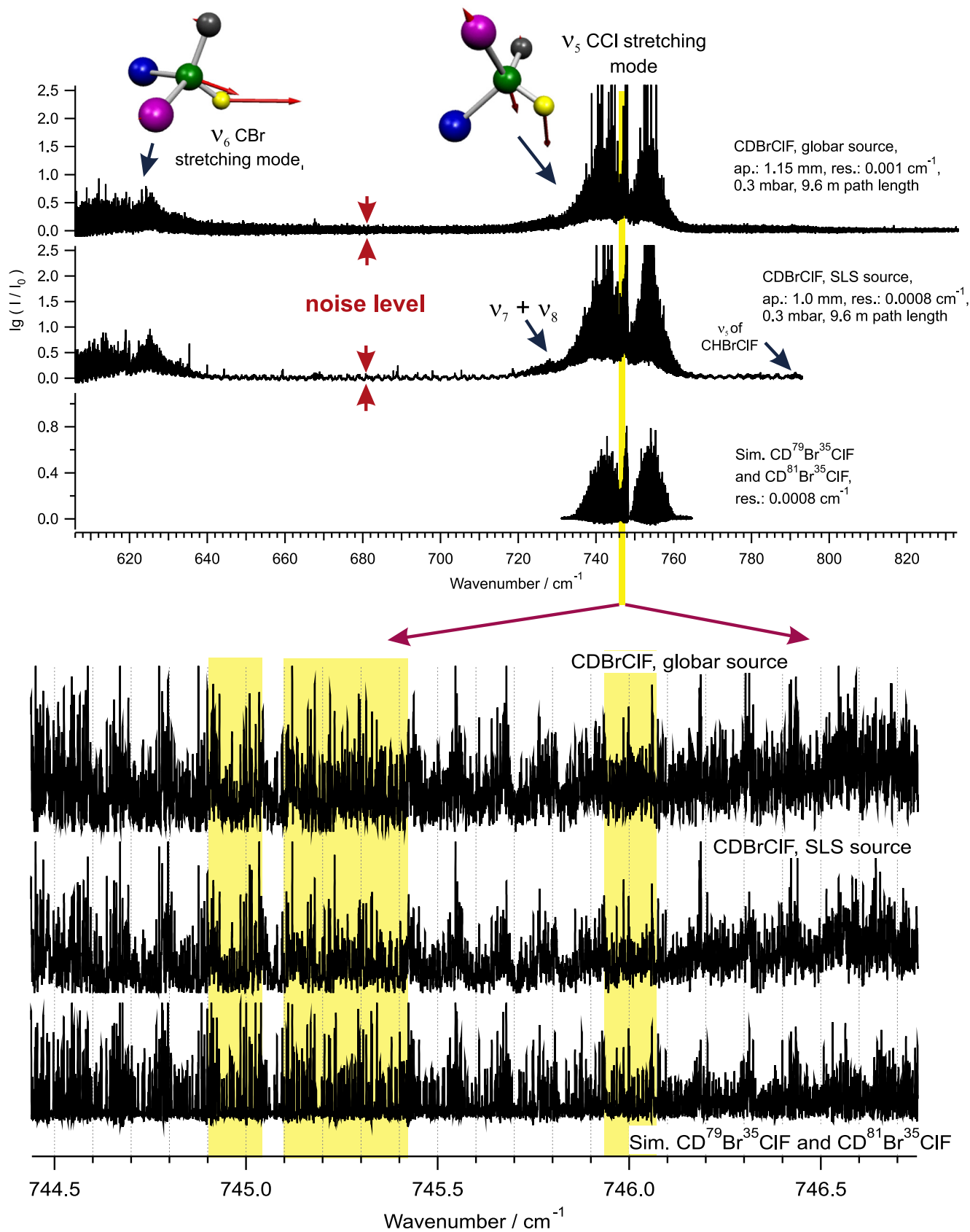
Fig. 7. Top: Survey of the FTIR spectrum of (CDBrClF) in the range 610–830 cm^{-1} showing the bands of the CBr-and CCl-stretching modes. The upper trace displays the spectrum recorded with the globar and the middle trace the spectrum recorded with the SLS light source. The bottom trace shows a simulated spectrum of the CCl-stretching band. The lower part shows an enlargement of the spectrum between 744.5 and 746.52 cm^{-1}.
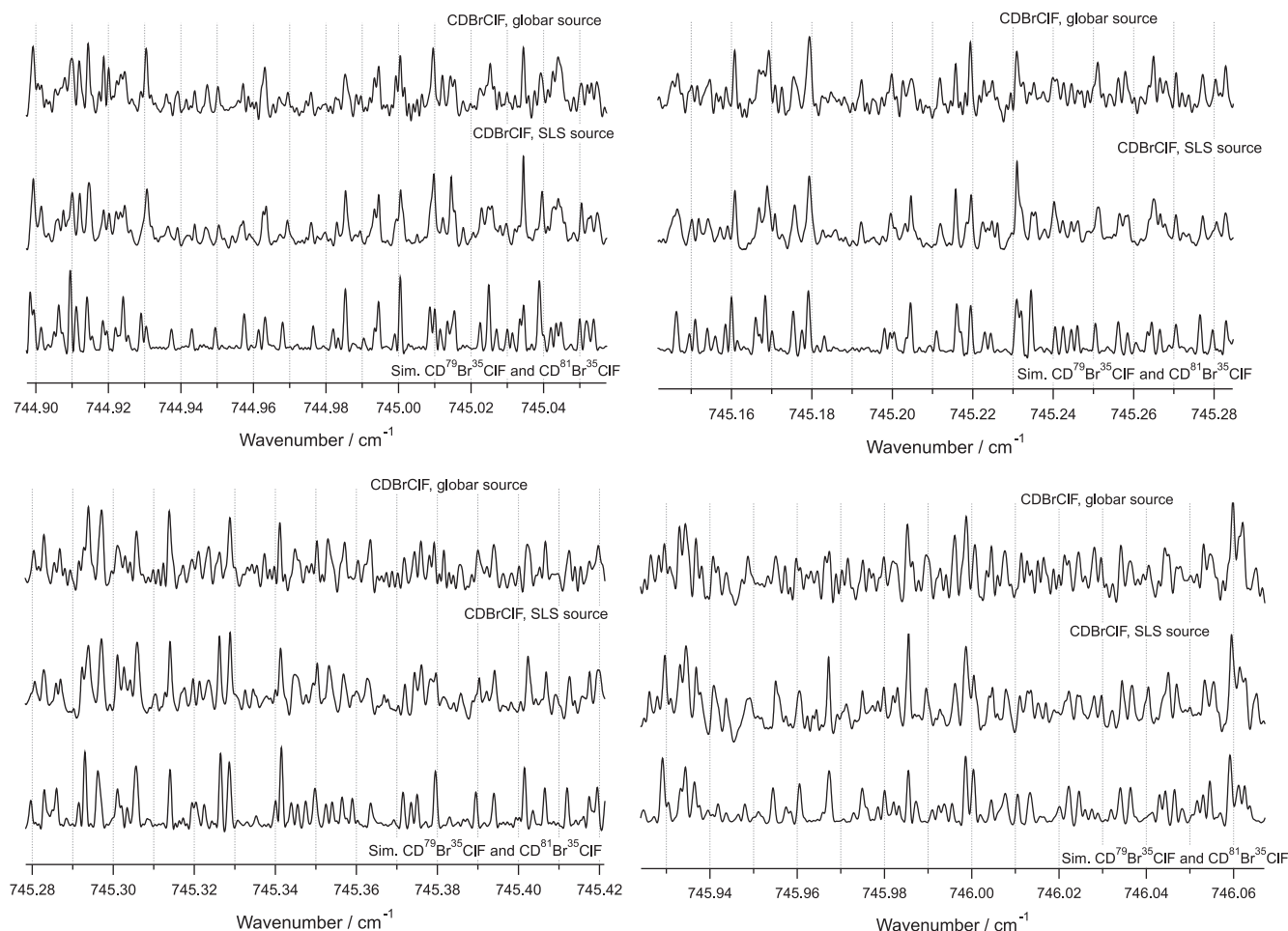
Fig. 8. Enlargements of the CDBrClF spectrum within the v_5 region shown in the lower part of Fig. 7.

Again, several series belonging to different isotopomers can be easily identified and assigned. The plot of the transitions against the rotational A constant is shown in the Loomis-Wood plot on the bottom left in Fig. 6 in which the different K_c series are visible. These b-type transitions coincide with c-type transitions and are grouped in four groups with $K_c + 4, 8, 12, \ldots$. These group patterns are different for $CD^{79}Br^{35}ClF$ and $CD^{81}Br^{35}ClF$. The transitions have been assigned up to $J \leqslant 105, K_a \leqslant 65$ and $K_c = 104$.

4. Rovibrational analysis and discussion

4.1. Effective Hamiltonian parameters

The rovibrational analysis has been carried out with Watson's A reduced effective Hamiltonians in the III^r representation using up to sextic centrifugal distortion constants [69]:

$$
\begin{aligned}
\widehat{H}_{rot}^{v,v} = &\, A_v \widehat{J}_z^2 + B_v \widehat{J}_x^2 + C_v \widehat{J}_y^2 \\
&- \Delta_J^v \widehat{J}^4 - \Delta_{JK}^v \widehat{J}^2 \widehat{J}_z^2 - \Delta_K^v \widehat{J}_z^4 \\
&- \frac{1}{2}[(\delta_J^v \widehat{J}^2 + \delta_K^v \widehat{J}_z^2), (\widehat{J}_+^2 + \widehat{J}_-^2)]_+ \\
&+ \Phi_J^v (\widehat{J}^2)^3 + \Phi_{JK}^v (\widehat{J}^2)^2 \widehat{J}_z^2 + \Phi_{KJ}^v \widehat{J}^2 \widehat{J}_z^4 + \Phi_K^v \widehat{J}_z^6 \\
&+ \frac{1}{2}[(\phi_J^v (\widehat{J}^2)^2 + \phi_{JK}^v \widehat{J}^2 \widehat{J}_z^2 + \phi_K^v \widehat{J}_z^4), (\widehat{J}_+^2 + \widehat{J}_-^2)]_+
\end{aligned}
\tag{1}
$$

The angular momentum operators are given by $\widehat{J}^2 = \widehat{J}_x^2 + \widehat{J}_y^2 + \widehat{J}_z^2$ and $\widehat{J}_\pm = \widehat{J}_x \pm i\widehat{J}_y$. The I^r representation was chosen to reduce correla-

tions during the fit. The spectroscopic data were analyzed using the WANG program described in detail in [70] (see also [63]). Each K_a or K_c subseries was successively included into the fit. The spectroscopic constants were defined and adjusted according to the A reduction.

4.2. Rovibrational analysis of the ground state of $CD^{79}Br^{35}ClF$ and $CD^{81}Br^{35}ClF$

There were no spectroscopic ground state constants available for any of the isotopomers of CDBrClF. For that reason combination differences (CD) have been calculated from the assigned transitions of the v_5, v_3 and v_4 fundamentals of $CD^{79}Br^{35}ClF$ and $CD^{81}Br^{35}ClF$. In a first step, these CD have been used to determine the ground state spectroscopic constants of $CD^{79}Br^{35}ClF$ and $CD^{81}Br^{35}ClF$. However, only 3000 CD have been used, less than half of the actually assigned transitions. In order to improve the higher order constants of the ground state and use the J quantum number up to 110, all assigned transitions of all assigned bands have been fitted together. The data set for adjusting the ground state constants was considerably enlarged as a result. Around 6000 transitions have been used to determine the rotational constants A, B, C, the quartic and sextic centrifugal distortions constants $\Delta_J, \Delta_{JK}, \Delta_K, \delta_J, \delta_K$ and Φ_J, ϕ_J and ϕ_K for $CD^{79}Br^{35}ClF$ as well as $A, B, C, \Delta_J, \Delta_{JK}, \Delta_K, \delta_J, \delta_K$ and $\Phi_J, \phi_J, \phi_{JK}$ and ϕ_K for $CD^{81}Br^{35}ClF$, according to Tables 2 and 3. Perturbed transitions have not been used for the fitting procedure.
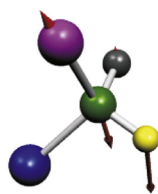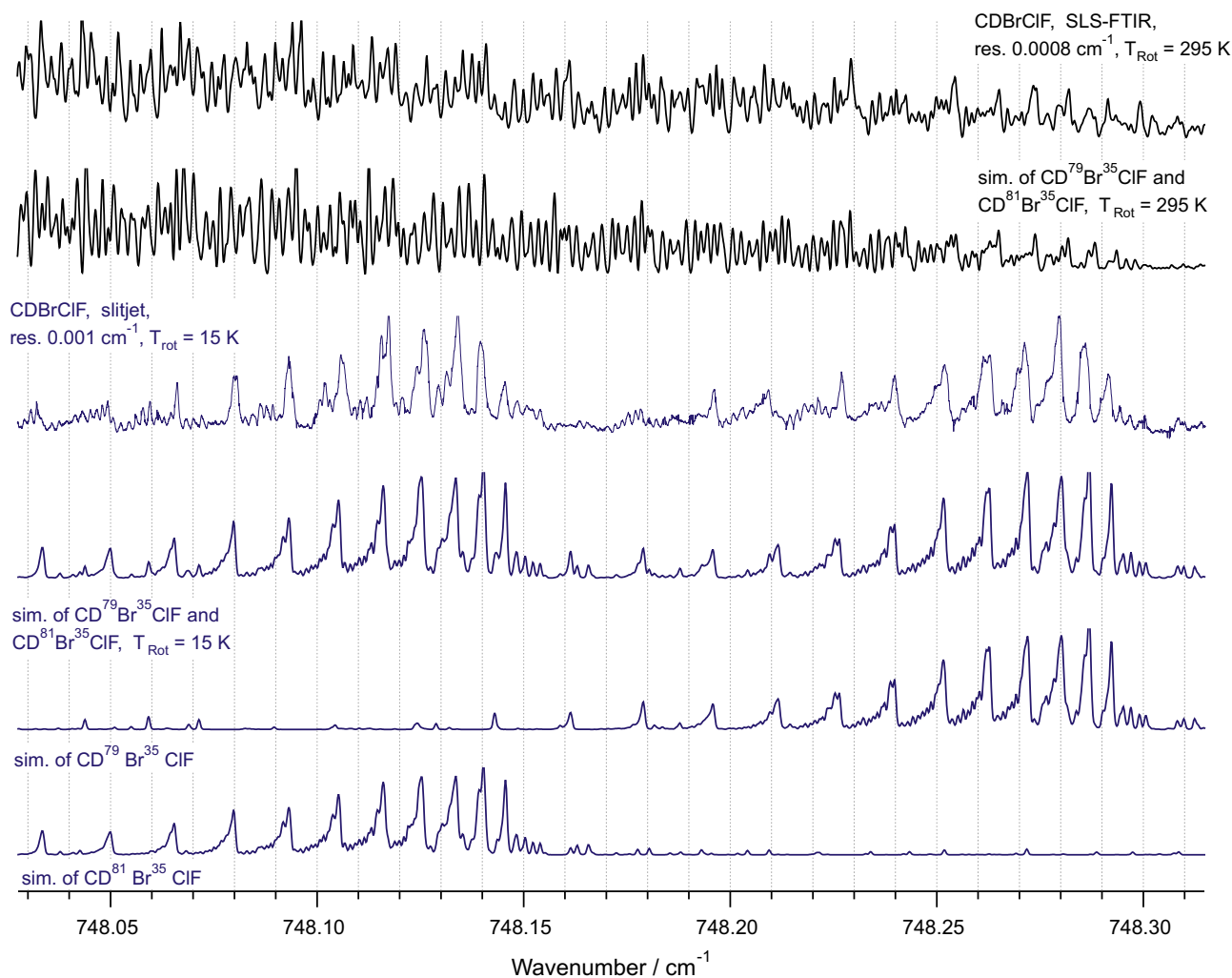
Fig. 9. The Q branch region of the v_5 fundamental of CDBrClF. Upper trace: The experimental spectrum of CDBrClF measured with the ETH-SLS FTIR spectrometer using synchrotron radiation at room temperature. Second trace: The simulated sum spectrum of $CD^{79}Br^{35}ClF$ and $CD^{81}Br^{35}ClF$ at 295 K. Third trace: The experimental spectrum of CDBrClF measured at 15 K with a jet-diode laser setup. Fourth trace: The simulated spectrum of $CD^{79}Br^{35}ClF$ and $CD^{81}Br^{35}ClF$ at 15 K. Fifth trace: Simulated spectrum of $CD^{79}Br^{35}ClF$ at 15 K. Last trace: Simulated spectrum of $CD^{81}Br^{35}ClF$ at 15 K.

4.3. Rovibrational analysis of the v_5 state of $CD^{79}Br^{35}ClF$ and $CD^{81}Br^{35}ClF$

The spectroscopic constants of the v_5 state of $CD^{79}Br^{35}ClF$ and $CD^{81}Br^{35}ClF$ have first been determined from the SLS-FTIR data set. Each of the different K_a series has been subsequently added to the fit. Based on the adjusted spectroscopic constants of the v_5 state the spectrum was simulated and compared to the cold spectrum measured with the diode laser supersonic jet setup. Additional lines at low J values in the Q and R branch region have been assigned and added in the fitting procedure. During the final adjustment of the constants the spectroscopic constants of the ground state of $CD^{79}Br^{35}ClF$ and $CD^{81}Br^{35}ClF$ were fixed to the values listed in Table 2 and 3 to reduce correlations, because only a-type transitions were used. Therefore, the uncertainty of the C rotational constant is smaller than that of the A and B constants. The final adjusted constants of the v_5 state of $CD^{79}Br^{35}ClF$ and $CD^{81}Br^{35}ClF$ are also listed in Tables 2 and 3.

A comparison of the rotational constants of the ground state with those of the v_5 state illustrates that exciting the CCl stretching mode decreases the A and C constants whereas the B constant changes much less. In the next step the spectrum was simulated on the basis of the adjusted constants. A comparison of the SLS-FTIR (upper trace) and globar FTIR (middle trace) measured spectrum with a simulated sum spectrum of the two major isotopomers $CD^{79}Br^{35}ClF$ and $CD^{81}Br^{35}ClF$ (lower trace) is shown in Figs. 7 and 8. As the extended spectral region in the P branch region in Fig. 8 illustrates, the agreement of the simulated (lower trace)
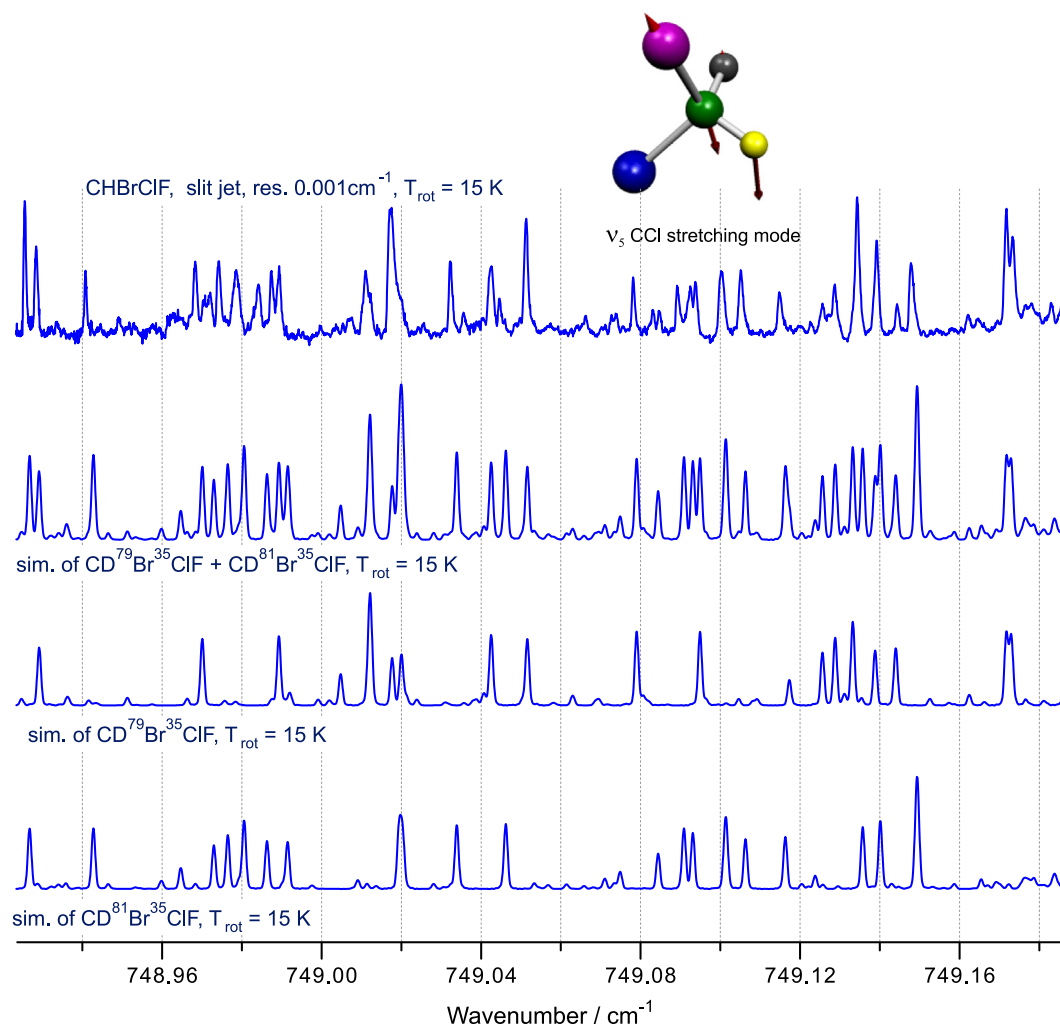
Fig. 10. Part of the R branch region of the ν_5 fundamental of CDBrClF. Upper trace: The experimental spectrum of CDBrClF measured at 15 K with a jet-diode laser setup. Second trace: The simulated spectrum of $CD^{79}Br^{35}ClF$ and $CD^{81}Br^{35}ClF$ at 15 K. Third trace: Simulated spectrum of $CD^{79}Br^{35}ClF$ at 15 K. Last trace: Simulated spectrum of $CD^{81}Br^{35}ClF$ at 15 K.

and recorded SLS-FTIR spectrum (middle trace) is relatively good. Of course, it is not perfect because the simulation does not include hot bands or transitions associated with the two other isotopomers $CD^{79}Br^{37}ClF$ and $CD^{81}Br^{37}ClF$. The influence of a higher noise level in a highly resolved experimental spectrum can be studied by comparison of the SLS-FTIR with the globar FTIR spectrum. The noise peaks in the globar FTIR spectrum (upper traces, Fig. 8) are sometimes of similar magnitude as the absorption lines. Only through comparison with the SLS-FTIR spectrum shown in the middle traces of Fig. 8 is it possible to make an assignment of the absorption line.

The advantage of cold jet spectra is shown in Fig. 9. Due to the low temperature of 15 K it was possible to partially resolve the Q branch at least with regard to the J quantum number of the CDBrClF spectrum. The Q branches of $CD^{79}Br^{35}ClF$ and $CD^{81}Br^{35}ClF$ are well separated, as the jet spectrum (third trace) in Fig. 9 illustrates. A comparison with a simulated sum spectrum (fourth trace) of $CD^{79}Br^{35}ClF$ (fifth trace) and $CD^{81}Br^{35}ClF$ (sixth trace) in Fig. 9 shows good agreement. In addition, we have added the SLS-FTIR spectrum of CDBrClF as the first trace in Fig. 9. The different Q branches of $CD^{79}Br^{35}ClF$ and $CD^{81}Br^{35}ClF$ are not visible in this SLS-FTIR spectrum recorded at 298 K. However, the agreement between the measured SLS-FTIR spectrum and a simulation of the sum of the calculated spectrum of $CD^{79}Br^{35}ClF$ and $CD^{81}Br^{35}ClF$

shown in the second trace of Fig. 9 is quite good. A reason for this nice agreement is the high resolution of around 25 MHz of the experimental spectrum. Due to high resolution the K_a absorption features are resolved and can therefore be more easily simulated. These features are not resolved in the jet spectrum. A part of the R branch region has also been measured with the jet diode laser setup and is shown in Fig. 10 (upper trace). In order to determine the rotational temperatures the spectrum was simulated at several rotational temperatures. The simulations with T_{rot}= 15 K are displayed in Fig. 10, in which the lower trace is a simulation of $CD^{81}Br^{35}ClF$, the third trace a simulation of $CD^{79}Br^{35}ClF$ and the second trace the sum of the simulations in the third and lower trace. The overall agreement with the experimental spectrum is good. This part of the R branch represents the transitions from $J = 6$ to $J = 7$. Here, the asymmetry splitting is large and completely resolved.

4.4. Rovibrational analysis of the ν_3 state of $CD^{79}Br^{35}ClF$ and $CD^{81}Br^{35}ClF$

The vibrational analysis of the ν_3 and $\nu_6 + \nu_8$ bands at modest resolution [44] has lead to the identification of an anharmonic resonance between these states. The locally perturbed K_a series of the ν_3 fundamental and $\nu_6 + \nu_8$ band between $J = 70 - 85$ for $CD^{79}Br^{35}ClF$ and between $J = 65 - 80$ for $CD^{81}Br^{35}ClF$ are due to

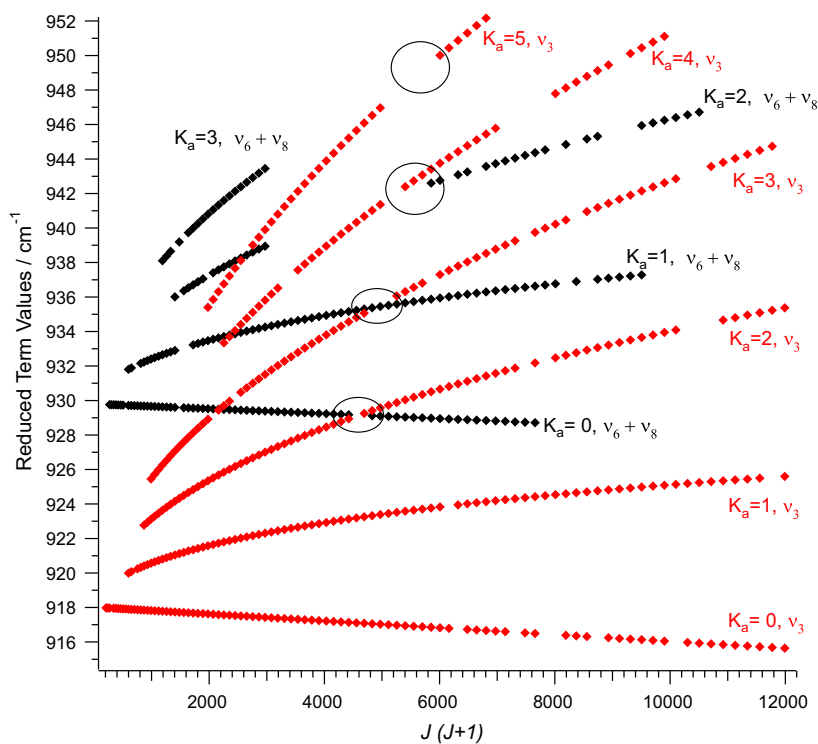**Fig. 11.** Reduced term values of the v_3 and $v_6 + v_8$ states of the $CD^{81}Br^{35}ClF$ isotopomer.
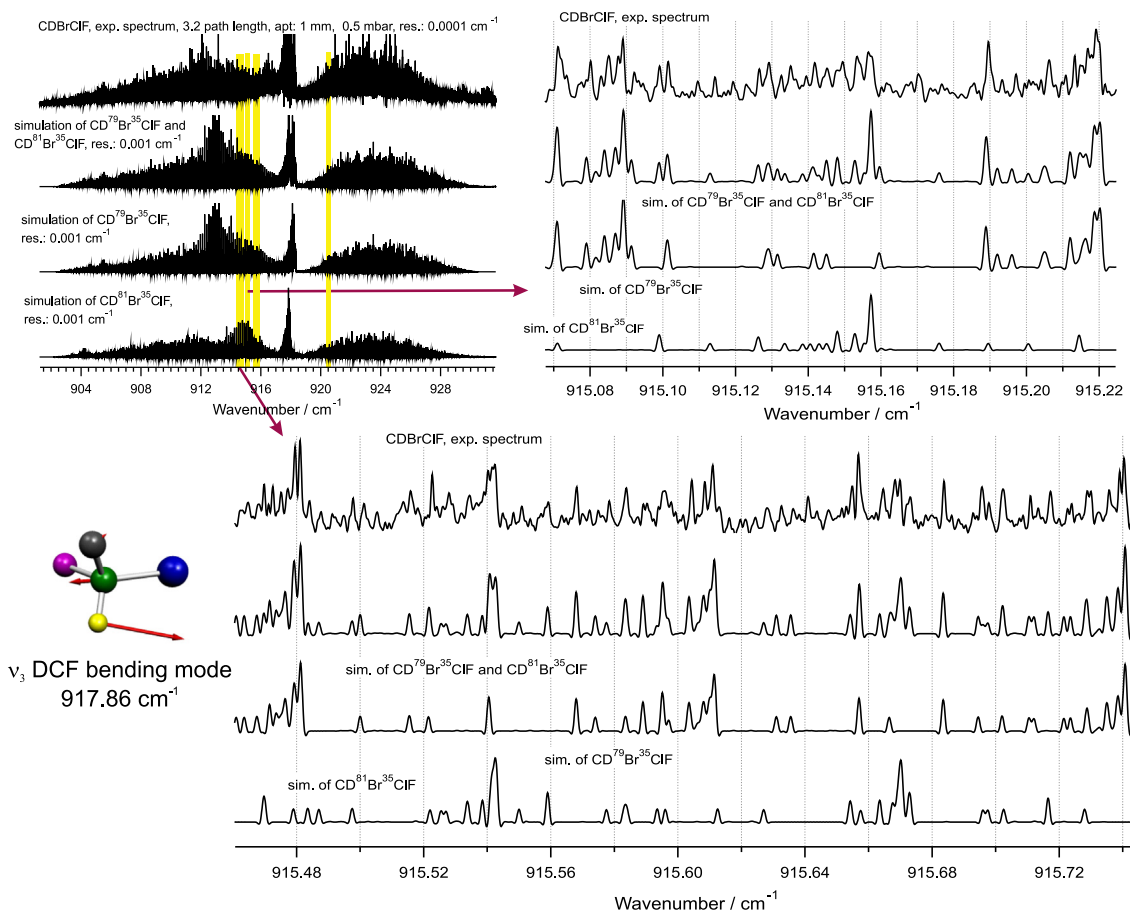

Fig. 12. Top left: Survey of the FTIR spectrum of (CDBrClF) in the range of the v_3 fundamental between 904 and 928 cm^{-1}. The upper trace displays the spectrum recorded with the globar source and the second trace shows the simulated sum spectrum of $CD^{79}Br^{35}ClF$ and $CD^{81}Br^{35}ClF$ at 295 K. The third and lower traces show the simulated spectra of $CD^{79}Br^{35}ClF$ (third) and $CD^{81}Br^{35}ClF$ (lower). Enlargements of the yellow shaded areas are shown on the top right and on the lower part and in Fig. 13. (For interpretation of the references to colour in this figure legend, the reader is referred to the web version of this article.)
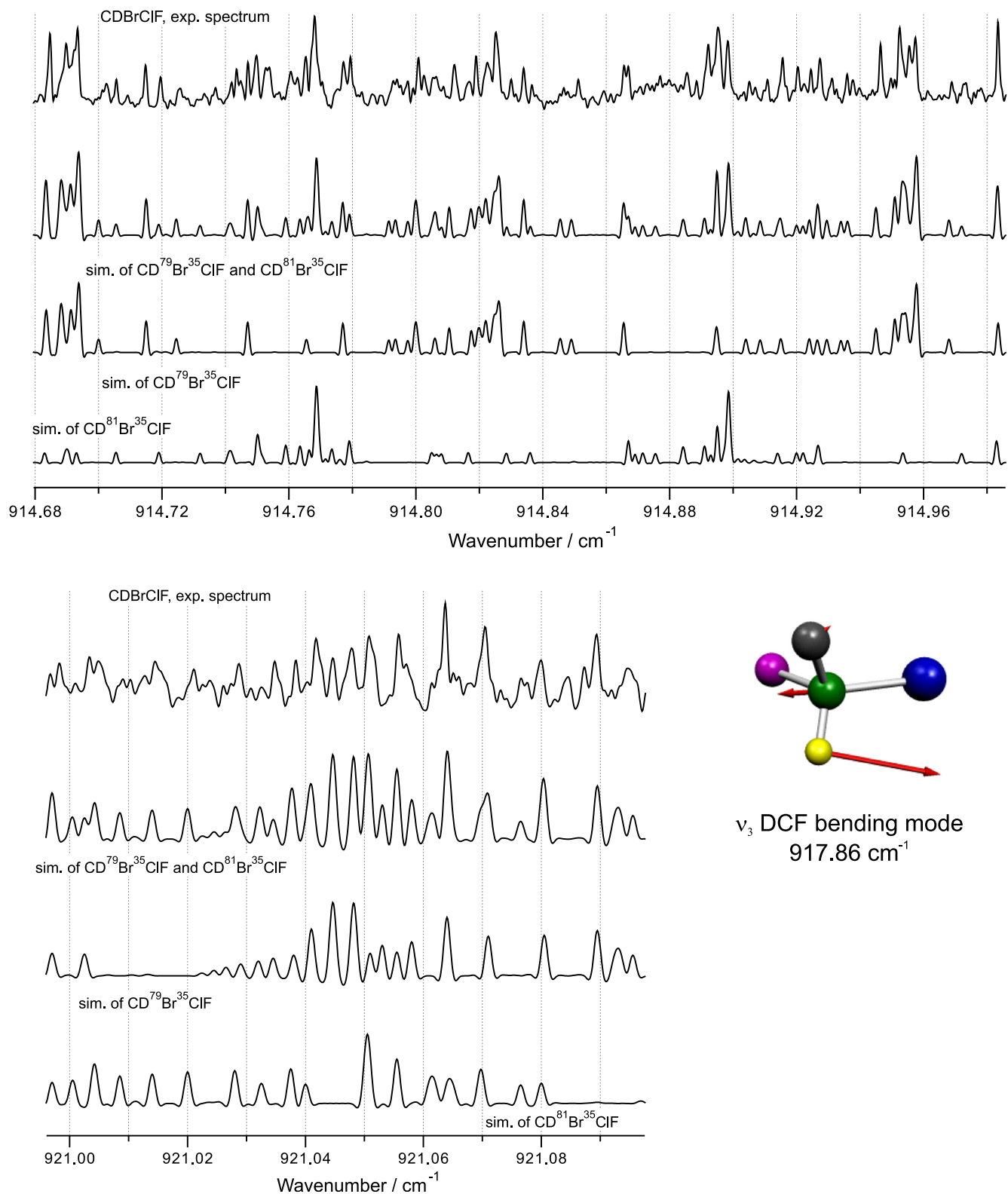
ν_3 DCF bending mode
917.86 cm^{-1}

Fig. 13. Top and bottom: Enlargements of the CDBrClF spectrum within the ν_3 region shown in the upper part of Fig. 12.

crossings of the $\Delta K_a = 2$ levels, which are nicely illustrated in the plot of the reduced term values for CD^{81}Br^{35}ClF shown in Fig. 11. The reduced term values are calculated by subtraction of the term values of the $K_a = 0$ levels of the ν_3 state from the measured lines. As one can see the term value differences between the $\Delta K_a = 0$ rovibrational levels of the ν_3 and $\nu_6 + \nu_8$ states do not change at all with increasing J number. This means that the two states have a similar C rotational constant. However, there are crossings of the $\Delta K_a = 2$ levels observed as local perturbations in the spectrum and in the Loomis-Wood diagrams of the ν_3 and $\nu_6 + \nu_8$ bands (Fig. 5, lower part). In addition, one recognizes crossings of $\Delta K_a = 3$ levels. However, there is no perturbation detected in the

Table 2

Spectroscopic constants in cm^{-1} of the ground state, the ν_5, ν_3 and ν_4 states of CD^{79}Br^{35}ClF with uncertainties listed as 1σ in parentheses in terms of the last significant digit [77]. If no uncertainties are listed, the constant was fixed during the fit.

	Ground state	ν_5	ν_3 (perturbed)[a]	ν_3 (deperturbed)[b]	$\nu_6 + \nu_8$ (deperturbed)[b]	ν_4
$\bar{\nu}_0$ (cm^{-1})	0	748.299792 (33)	918.371542 (58)	918.630 (33)	931.231 (33)	1082.811560 (19)
A (cm^{-1})	0.20870462 (52)	0.2080009 (73)	0.2084316 (42)	0.2084431 (19)	0.207750 (34)	0.20797335 (51)
B (cm^{-1})	0.0672532 (21)	0.06721366 (40)	0.0671144 (21)	0.06711403 (24)	0.0671802 (28)	0.0672373 (21)
C (cm^{-1})	0.05325952 (34)	0.05318766 (12)	0.05305212 (47)	0.05305072 (19)	0.05311659 (20)	0.05323197 (33)
$\Delta_J/10^{-6}$ (cm^{-1})	0.11359 (45)	0.114 (40)	0.0808 (35)	0.07575 (33)	0.163 (13)	0.11307 (43)
$\Delta_{JK}/10^{-6}$ (cm^{-1})	−0.3046 (17)	−0.3046	−0.188 (12)	−0.1771 (18)	−0.169 (15)	−0.3020 (19)
$\Delta_K/10^{-6}$ (cm^{-1})	0.1969 (12)	0.197 (87)	0.1132 (89)	0.10692 (72)	0.0118 (11)	0.1948 (18)
$\delta_J/10^{-6}$ (cm^{-1})	0.05542 (28)	0.05542	0.0391 (17)	0.03672 (16)	0.0832 (13)	0.05528 (26)
$\delta_K/10^{-6}$ (cm^{-1})	−0.11553 (11)	−0.116 (51)	−0.0685 (45)	−0.06558 (41)		−0.1145 (14)
$\Phi_J/10^{-12}$ (cm^{-1})	−0.0250 (31)	−0.0235 (11)	−0.0227 (51)	0.02502 (49)		−0.0239 (28)
$\phi_J/10^{-12}$ (cm^{-1})	0.215 (12)	0.190 (38)	0.215 (35)	0.2295 (27)		0.219 (14)
$\phi_K/10^{-12}$ (cm^{-1})	−0.546 (30)	0.515 (22)	−0.498 (49)	−0.5403 (43)		−0.542 (33)
W (cm^{-1})					1.84 (0.11)	
N_{data}	4304	730	1070		1217	2644
d_{rms} (cm^{-1})	0.00020	0.00021	0.00037		0.00031	0.00021

[a] No interaction is considered and therefore lines within the crossing regions are not included in the fit.

[b] An anharmonic resonance with coupling matrix element W between ν_3 and $\nu_6 + \nu_8$ states is considered. The term value ν_3 ($J = 0$) = 918.3716 cm^{-1} agrees with the corresponding ν_0 (perturbed). One has also $\nu_6 + \nu_8$ ($J = 0$) = 931.4946 cm^{-1}.

Table 3

Spectroscopic constants in cm^{-1} of the ground state, the ν_5, ν_3 and ν_4 states of CD^{81}Br^{35}ClF with uncertainties listed as 1σ in parentheses in terms of the last significant digit [77]. If no uncertainties are listed, the constant was fixed during the fit.

	Ground state	ν_5	ν_3 (perturbed)[a]	ν_3 (deperturbed)[b]	$\nu_6 + \nu_8$ (deperturbed)[b]	ν_4
$\bar{\nu}_0$ (cm^{-1})	0	748.154143 (31)	918.020628 (56)	918.58 (14)	929.24 (12)	1082.796290 (22)
A (cm^{-1})	0.20856065 (55)	0.207846 (21)	0.2082908 (59)	0.2082736 (66)	0.208619 (85)	0.20783003 (56)
B (cm^{-1})	0.0665843 (19)	0.0665449 (17)	0.0664436 (23)	0.06644417 (39)	0.0664523 (65)	0.0665686 (20)
C (cm^{-1})	0.05282134 (36)	0.05274967 (34)	0.05261951 (44)	0.05261627 (91)	0.0526844 (10)	0.05279410 (37)
$\Delta_J/10^{-6}$ (cm^{-1})	0.12355 (39)	0.0950 (68)	0.05963 (87)	0.0561 (70)	0.105 (91)	0.12314 (42)
$\Delta_{JK}/10^{-6}$ (cm^{-1})	−0.3438 (15)	−0.341 (23)	−0.0986 (31)	−0.0827 (98)	−0.315 (87)	−0.3417 (17)
$\Delta_K/10^{-6}$ (cm^{-1})	0.2263 (12)	0.252 (16)	0.0448 (22)	0.0324 (76)	0.217 (95)	0.2246 (11)
$\delta_J/10^{-6}$ (cm^{-1})	0.05019 (24)	0.0337 (34)	0.0192 (44)	0.0173 (37)	0.041 (13)	0.04996 (22)
$\delta_K/10^{-6}$ (cm^{-1})	−0.11795 (24)	−0.134 (93)	−0.0166 (12)	−0.00940 (97)	−0.116 (83)	−0.11693 (23)
$\Phi_J/10^{-12}$ (cm^{-1})	0.00551 (31)	−0.00370 (64)	0.00769 (61)	0.00662 (53)		0.00583 (33)
$\phi_J/10^{-12}$ (cm^{-1})	0.187 (16)	0.134 (53)	0.172 (31)	0.179 (29)		0.182 (17)
$\phi_{JK}/10^{-12}$ (cm^{-1})	−0.631 (66)	−0.461 (92)	−0.548 (71)	−0.581 (68)		−0.620 (68)
$\phi_K/10^{-12}$ (cm^{-1})	0.500 (71)	0.321 (81)	−0.486 (41)	0.501 (40)		0.501 (73)
W (cm^{-1})					2.50 (0.30)	
N_{data}	4248	750	973		1160	2525
d_{rms} (cm^{-1})	0.00020	0.00021	0.00037		0.00031	0.00021

[a] No interaction is considered and therefore lines within the crossing regions are not included in the fit.

[b] An anharmonic resonance with coupling matrix element W between ν_3 and $\nu_6 + \nu_8$ states is considered. One has ν_3 ($J = 0$) = 918.0205 cm^{-1} and $\nu_6 + \nu_8$ ($J = 0$) = 929.7995 cm^{-1} (see also Table 2).

spectrum at this $\Delta K_a = 3$ crossing. $\Delta K_a = 1$ crossings are not observed within the range of the measured lines.

The analysis of the ν_3 state was performed according to two models. In the first model no interaction with $\nu_6 + \nu_8$ was considered. Lines within the local crossings were not included in the fitting procedure. The adjusted spectroscopic constants are listed in Tables 2 and 3 labeled as perturbed. The listed $\bar{\nu}_0$ corresponds to the effective observed band center in the spectra. The second model used took the anharmonic resonance into consideration. 2 cm^{-1} was used as a starting value for the coupling matrix element W which lead to an adjusted parameter of $W = 1.84$ cm^{-1} for CD^{79}Br^{35}ClF and of $W = 2.50$ cm^{-1} for CD^{81}Br^{35}ClF. The d_{rms} improved from 0.00037 cm^{-1} (first model) to 0.00031 cm^{-1} (second model). However, there were large correlations between W and the centers of the bands and therefore the uncertainty is relatively large, as shown in Tables 2 and 3. Due to the similar rotational constants of both interacting states it is fairly difficult to fit this $\Delta K_a = 0$ anharmonic resonance. Another disadvantage is the missing assignment of the P branches of the $\nu_6 + \nu_8$ band.

The fit is only carried out using R branch lines of the $\nu_6 + \nu_8$ band and therefore the correlations during the fit are higher. The coupling matrix elements W for the two isotopomers are 1.84 (11) cm^{-1} and 2.50 (30) cm^{-1} as compared to $W = 5.3$ cm^{-1} which was estimated in [44] with the assumption that $\nu_6 + \nu_8$ has no zero order intensity, which leads to an overestimate as a rule. We note that the ν_i (deperturbed) are formal parameters of the effective resonance Hamiltonian. The experimentally observable term values ν_i ($J = 0$) are given in the footnote as well and agree for both models within the uncertainties.

The spectrum of the ν_3 and $\nu_6 + \nu_8$ band was simulated using the deperturbed spectroscopic constants in Tables 2 and 3 and is displayed in Figs. 12 and 13. The measured ν_3 fundamental and $\nu_6 + \nu_8$ bands of CDBrClF are displayed in the upper trace of each panel in Figs. 12 and 13. The third and lower trace display a simulated spectrum of the CD^{79}Br^{35}ClF and CD^{81}Br^{35}ClF isotopomer and the second trace is the sum of the simulated spectrum of both isotopomers. On the top right and in the lower part, expanded regions of the P branch regions of ν_3 are shown.
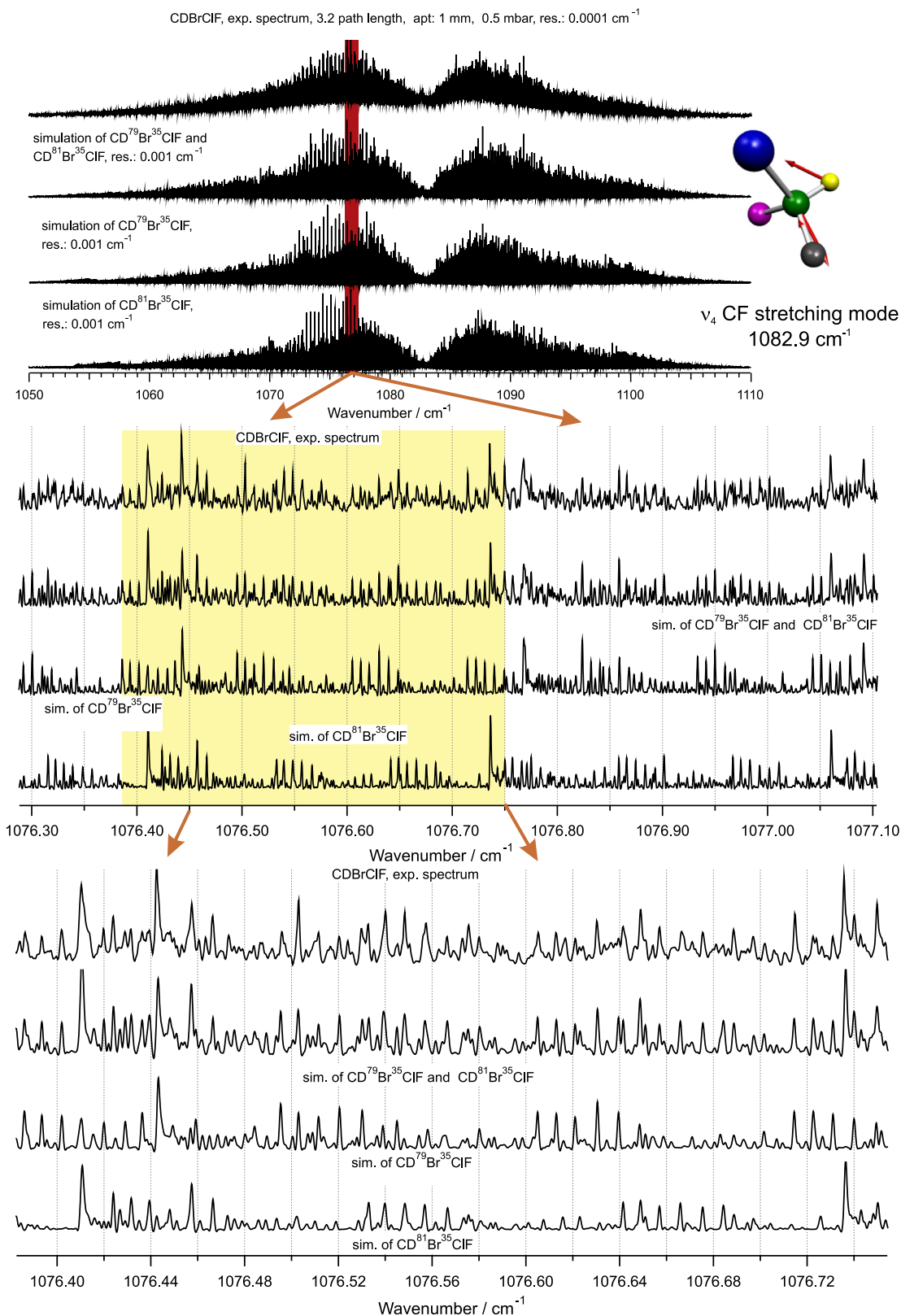
Fig. 14. Top: Survey of the FTIR spectrum of (CDBrClF) in the range of the v_4 fundamental between 1050 and 1110 cm^{-1}. The upper trace displays the spectrum recorded with the globar source and the second trace shows the simulated sum spectrum of CD^{79}Br^{35}ClF and CD^{81}Br^{35}ClF at 295 K. The third and lower traces show the simulated spectra of CD^{79}Br^{35}ClF (third) and CD^{81}Br^{35}ClF (lower). Middle: Enlargement of the red shaded area of the upper part. Bottom: Enlargement of the yellow shaded area of the middle part. (For interpretation of the references to colour in this figure legend, the reader is referred to the web version of this article.)

A comparison between the measured (upper trace) and simulated (second trace) spectra illustrates a good agreement. This is also true for the expanded spectral regions shown in Fig. 13. Here one observes in the upper part an expanded part of the v_3 P branch region, and in the lower part an expanded part of the R branch region.
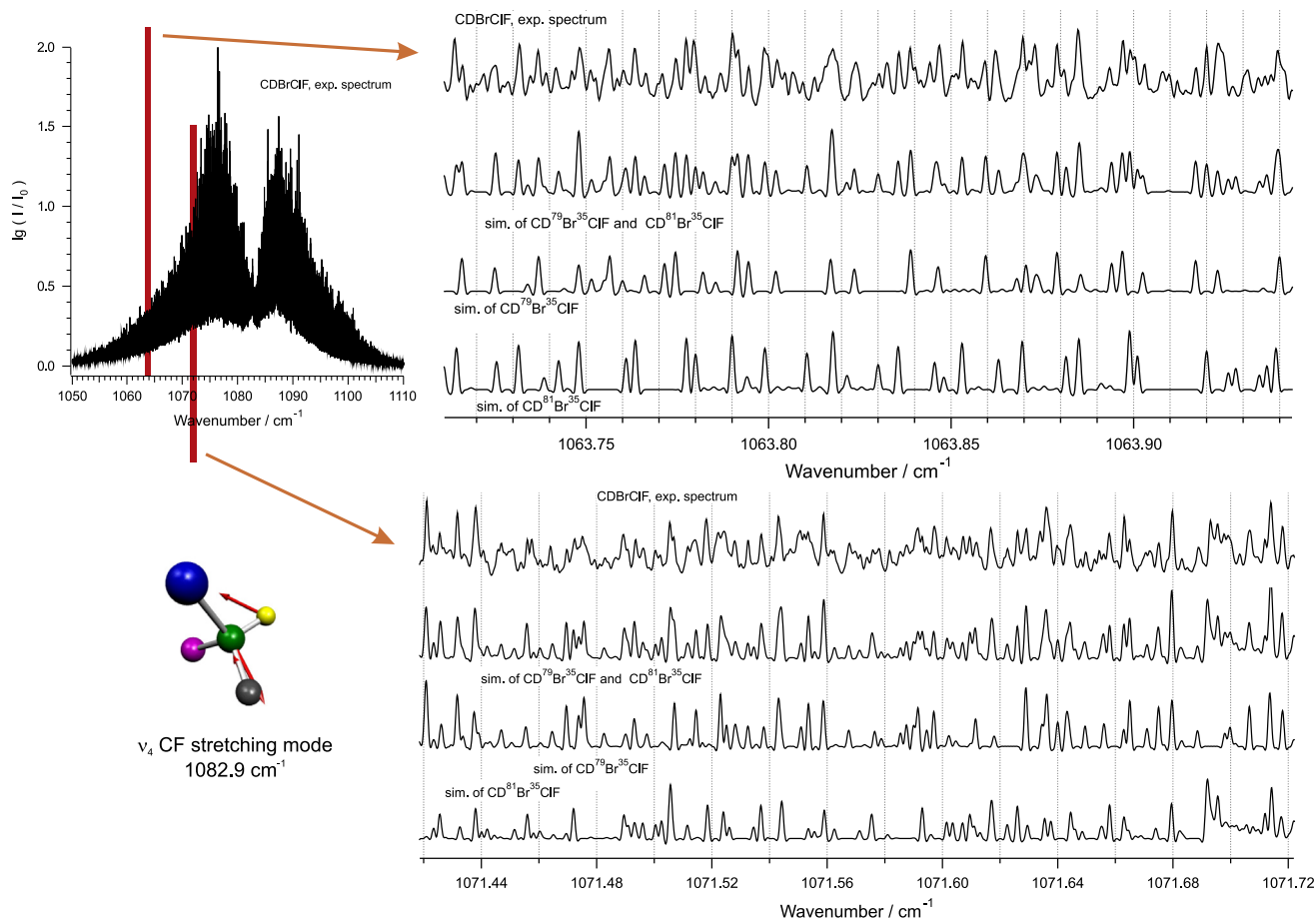
Fig. 15. Top and bottom: Enlargements of the P branch range of the ν_4 fundamental shown on the left. The upper trace displays the spectrum recorded with the globar source and the second trace shows the simulated sum spectrum of CD^{79}Br^{35}ClF and CD^{81}Br^{35}ClF at 295 K. The third and lower traces show the simulated spectra of CD^{79}Br^{35}ClF (third) and CD^{81}Br^{35}ClF (lower).

4.5. Rovibrational analysis of the ν_4 state of CD^{79}Br^{35}ClF and CD^{81}Br^{35}ClF

The ν_4 fundamental of CDBrClF is the CF-stretching mode and consists of b-type transitions which coincide partly with a-type and c-type transitions. There were no perturbations observed within the range of the observed transitions. As mentioned in Ref. [44] in agreement with theory the fundamental and harmonic wavenumber for the mode ν_4 of CDBrClF is at higher wavenumber ($\tilde{\nu} = 1082$ cm^{-1}) than that of CHBrClF ($\tilde{\nu} = 1077$ cm^{-1}). The shift of the ν_4 band center for the pair CD^{79}Br^{35}ClF/CD^{81}Br^{35}ClF (0.015 cm^{-1}) is slightly smaller than for the pair CH^{79}Br^{35}ClF/CH^{81}Br^{35}ClF (0.045 cm^{-1}).

The various assigned K_a and K_c series have been successively added to the fitting procedure. Finally, more than 4600 transitions of CD^{79}Br^{35}ClF and more than 5000 transitions of CD^{81}Br^{35}ClF have been used to adjust the spectroscopic constants of the ν_4 state of CD^{79}Br^{35}ClF and CD^{81}Br^{35}ClF. A comparison of the rotational constants of CD^{79}Br^{35}ClF and CD^{81}Br^{35}ClF for this state, shown in Tables 2 and 3 with the corresponding constants of the ground state, illustrates a decrease of the rotational constant A upon excitation of ν_4. The B and C rotational constants in the ground and excited states are similar. Based on the adjusted constants the ν_4 fundamental was simulated as displayed in Fig. 14. The upper left part shows the complete ν_4 fundamental, where the upper trace displays the recorded experimental spectrum of CDBrClF, the second trace the sum spectrum of the simulation of the CD^{79}Br^{35}ClF

and CD^{81}Br^{35}ClF isotopomers, the third trace the simulation of CD^{79}Br^{35}ClF and the fourth trace the simulation of CD^{81}Br^{35}ClF. The upper detailed part is an enlargement of the red marked region within the P branch range. This is the spectral region in which the b-type transitions coincide with a-type transitions. The regular structure of the absorption lines is clearly visible. The lower part is an expansion of the yellow shaded range near 1076.5 cm^{-1}. A comparison of the experimental spectrum (upper trace, lower part) with the simulation (second trace, lower part) illustrates the very good agreement, although absorption lines of hot bands and of isotopomers CD^{79}Br^{37}ClF and CD^{81}Br^{37}ClF are not considered in the simulation.

Fig. 15 illustrates other parts of the P branch region of ν_4. The b-type transitions coincide in this region with c-type transitions. Again, the agreement between simulation and experimental spectrum even at high J values is quite good as illustrated in the lower part. The same is true for the R branch region of ν_4 shown in Fig. 16 in which the b-type transitions coincide with a-type transitions and in Fig. 17 in which the b-type transitions coincide with c-type transitions. We have also assigned about 500 lines of the $2\nu_4$ overtone, for which a preliminary band center at 2145.1 cm^{-1} can be derived. This band is strongly perturbed.

5. Conclusions

We have presented a high resolution rovibrational analysis of the spectra of the chiral molecule CDBrClF in the infrared region covering three fundamental bands in the range 600–1100 cm^{-1}.
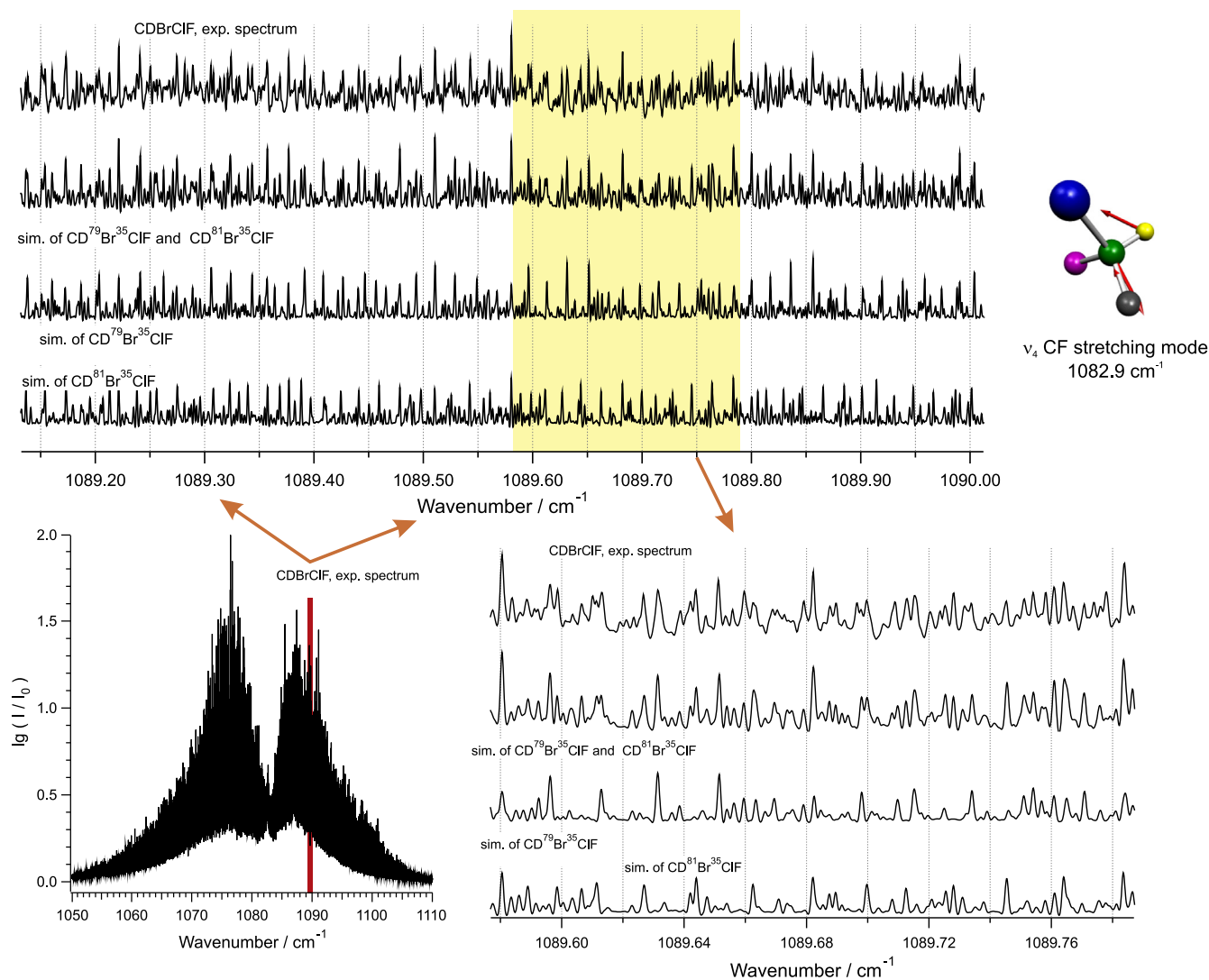
Fig. 16. Enlargements (top and bottom right) of the R branch range of the v_4 fundamental shown on the bottom left. The upper trace displays the spectrum recorded with the globar source and the second trace shows the simulated sum spectrum of CD^{79}Br^{35}ClF and CD^{81}Br^{35}ClF at 295 K. The third and lower traces show the simulated spectra of CD^{79}Br^{35}ClF (third) and CD^{81}Br^{35}ClF (lower).

The analysis illustrates that a systematic investigation of the rovibrationally resolved infrared spectrum is possible for this complicated chiral molecule, even at room temperature, if highly resolving spectrometers like the Bruker prototype spectrometers in combination with a powerful source like a synchrotron are used. However, with laser spectroscopy of molecules cooled in a supersonic jet, the spectral analysis is considerably simplified, as the assignment of the v_5 bands illustrates, even if the resolution is slightly worse due to the laser bandwidth in this case.

Only a-type transitions of the v_3 and v_5 bands have been assigned because the expected c-type transitions are too weak to be detected. Therefore, the A and B rotational constants are less well determined than the C constant of these two levels, as opposed to the v_4 fundamental consisting of b-type transitions. For these bands all three rotational constants are well determined because part of the b-type transitions coincide with a-type and c-type transitions. However, we have not yet detected an asymmetry splitting within these three bands measured at room temperature, so far we have only identified the splitting in the jet-cooled spectra of v_5.

The high resolution results of the present work are of importance for two broader areas of intramolecular dynamics. One of these aspects concerns intramolecular vibrational energy redistribution and energy flow. Spectroscopy in the mid infrared and near infrared at lower resolution has shown that the four high frequency modes v_1, v_2, v_3, v_4 form a four dimensional subspace of strongly coupled vibrations through dominant anharmonic resonances, where efficient energy flow occurs on a time scale of a few hundred fs [44]. Very little is known so far about the coupling to the set of lower frequency modes which presumably becomes important on longer time scales. The present analysis of the v_3, v_4 and v_5 fundamentals provides a first step towards future studies of the weaker couplings of the higher frequency modes to the lower frequency modes in CDBrClF as a possible prototype for IVR in chiral molecules [9,21–23,44]. The $v_6 + v_8/v_3$ resonance system is an example of that and illustrates how an anharmonic resonance with $\Delta K_a = 0$ and $\Delta K_a = 2$ interactions can be analyzed. A coupling matrix element of about 2 cm^{-1} (depending upon isotopomer) results in a time scale of about 10 ps for the redistribution of energy from the "high frequency" mode v_3 to the low
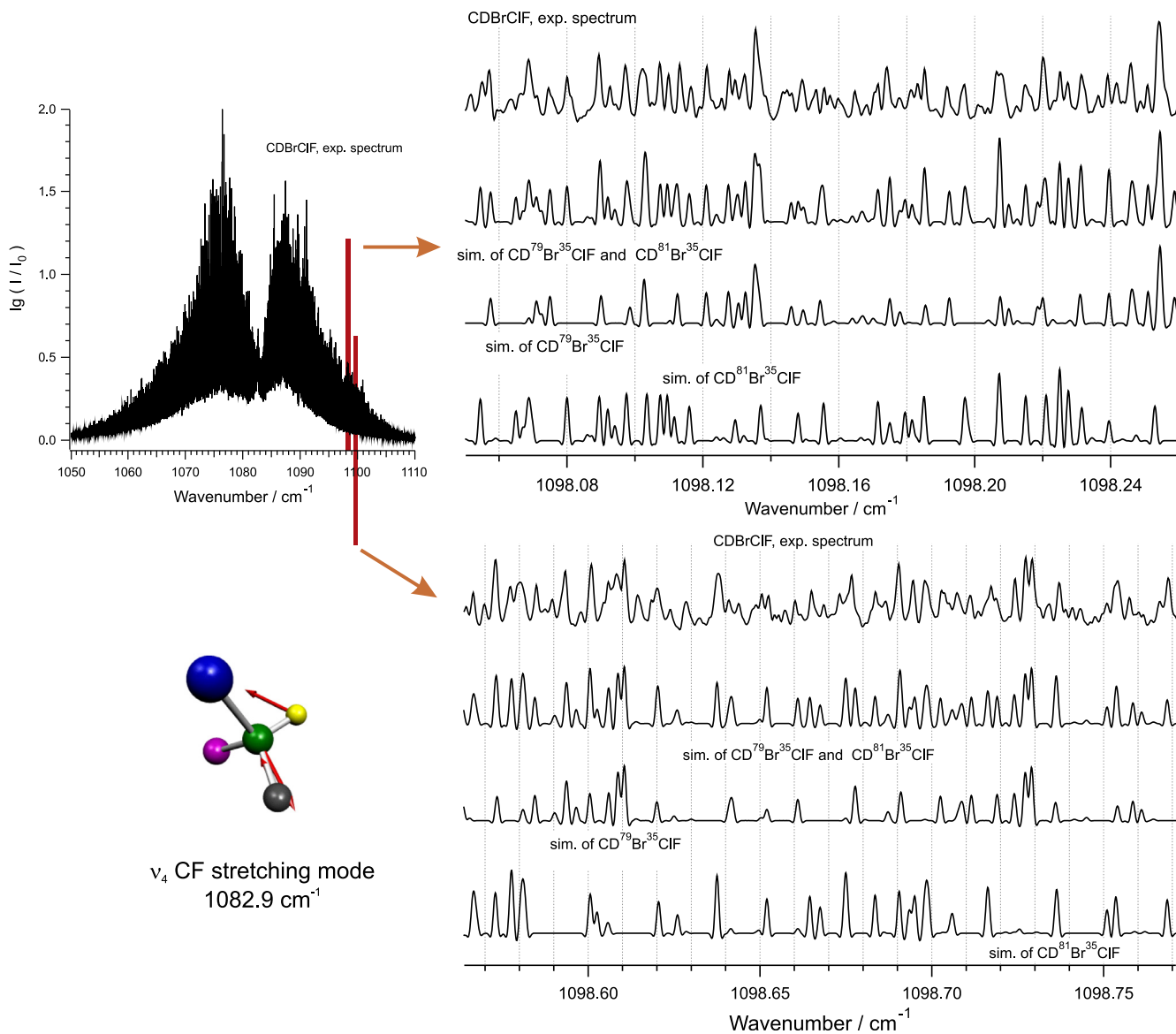
Fig. 17. Enlargements (top right and bottom right) of the R branch range of the v_4 fundamental shown on the top left. The upper trace displays the spectrum recorded with the globar source and the second trace shows the simulated sum spectrum of CD^{79}Br^{35}ClF and CD^{81}Br^{35}ClF at 295 K. The third and lower traces show the simulated spectra of CD^{79}Br^{35}ClF (third) and CD^{81}Br^{35}ClF (lower).

frequency modes $v_6 + v_8$. This can be compared to the 100 fs time scales for redistribution among the high frequency modes [44].

Another fundamental intramolecular process happening on a much longer time scale is the change of parity, requiring seconds in isolated chiral molecules [18,71]. This process results from the electroweak parity violation in chiral molecules which has been theoretically predicted but so far never observed experimentally. A search for possible prototype molecules for current experimental efforts is important in this context. CHBrClF might be used with a scheme involving achiral excited electronic states, if these can be identified [71], or else it can be used with a different scheme attempting to measure parity violation by means of infrared line shifts between the two enantiomers [10,18,20,24–28,72]. Indeed, CDBrClF has already been selected for protypical studies of the effect of anharmonic vibrational couplings on both the ground state energy differences $\Delta_{PV}E$ between enantiomers and frequency shifts in symmetrically equivalent infrared lines of enantiomers [28].

Considering line shift experiments for the detection of parity violation we can recommend b-type transitions coinciding with a-type transitions of the v_4 band because these lines are partly resolved with regard to their K_a substructure. Using our rovibrational analysis one should resolve and analyze the quadrupole splitting in a next step as described in [10,24] and then one could look for coincidences with CO_2 laser lines (9.4 μm emission band), as outlined in [10] for CHBrClF. Ultrahigh resolution spectroscopy using CW-CO_2 laser lines would not yet be able to detect line shifts due to parity violation which are predicted to be on the order of $\delta v/v = 10^{-16}$ [25–28] depending on the vibrational level considered. Current resolution limits in the most recent experiments are on the order of 10^{-13} to 10^{-14} [72]. However, future improvements may make smaller line shifts measurable either for CDBrClF or else other molecules can be considered where the effects are larger. Whatever route will be taken in the future of these experiments, high resolution spectroscopic analyses of the kind presented here provide a necessary first step. Indeed, the effective

Hamiltonian parameters derived here are sufficient to generate tables of line coincidences with CO_2 laser lines for ultra-precise studies, similar to the tables presented for CHBrClF [10]. Finally CDBrClF might also be a useful prototype molecule for the application of the Hirota approach towards microwave spectroscopy of chiral molecules [73,74] and chiral recognition [1,75,76].

Acknowledgements

Appendix A. Supplementary material

Supplementary data associated with this article can be found, in the online version, at http://dx.doi.org/10.1016/j.jms.2017.03.004.

References

[1] W. Caminati, Microwave spectroscopy of large molecules and molecular complexes, in: M. Quack, F. Merkt (Eds.), Handbook of High Resolution Spectroscopy, vol. 2, John Wiley & Sons, Ltd, Chichester, 2011, pp. 829–852 (Chapter 21).
[2] J.-U. Grabow, Fourier transform microwave spectroscopy measurement and instrumentation, in: M. Quack, F. Merkt (Eds.), Handbook of High Resolution Spectroscopy, vol. 2, John Wiley & Sons, Ltd, Chichester, 2011, pp. 723–799 (Chapter 19).
[3] S.T. Shipman, B.H. Pate, New techniques in microwave spectroscopy, in: M. Quack, F. Merkt (Eds.), Handbook of High Resolution Spectroscopy, vol. 2, John Wiley & Sons, Ltd, Chichester, 2011 (Chapter 20).
[4] P. Ottaviani, A. Maris, W. Caminati, J. Mol. Struct. 695–696 (2004) 353–356.
[5] W. Caminati, G. Maccaferri, P.G. Favero, L.B. Favero, Chem. Phys. Lett. 251 (1996) 189–192.
[6] S. Blanco, M.E. Sanz, J.C. Lopez, J.L. Alonso, Proc. Natl. Acad. Sci. 104 (2007) 20183–20188.
[7] J.P.I. Hearn, R.V. Cobley, B.J. Howard, J. Chem. Phys. 123 (2005) 134324.
[8] N. Borho, Y. Xu, Angew. Chem. Int. Ed. 46 (2007) 2276–2279.
[9] A. Beil, D. Luckhaus, R. Marquardt, M. Quack, J. Chem. Soc. Faraday Discuss. 99 (1994) 96–97. and 49–76.
[10] A. Bauder, A. Beil, D. Luckhaus, F. Müller, M. Quack, J. Chem. Phys. 106 (1997) 7558–7570.
[11] H. Hollenstein, D. Luckhaus, J. Pochert, M. Quack, G. Seyfang, Angew. Chem. 109 (1997) 136–140.
[12] S. Albert, M. Quack, ChemPhysChem 8 (2007) 1271–1281.
[13] S. Albert, K. Keppler Albert, M. Quack, Trends Opt. Photon. 84 (2003) 177–180.
[14] S. Albert, K. Keppler Albert, M. Quack, High resolution Fourier transform infrared spectroscopy, in: M. Quack, F. Merkt (Eds.), Handbook of High Resolution Spectroscopy, vol. 2, Wiley, John Wiley & Sons, Ltd, 2011, pp. 965–1019 (Chapter 26).
[15] S. Albert, I. Bolotova, Z. Chen, C. Fabri, L. Horny, M. Quack, G. Seyfang, D. Zindel, Phys. Chem. Chem. Phys. 18 (2016) 21976–21993.
[16] S. Albert, M. Quack, Nachrichten Chem. 62 (2014) 313–318.
[17] M. Quack, J. Stohner, M. Willeke, Annu. Rev. Phys. Chem. 59 (2008) 741–769.
[18] M. Quack, Fundamental symmetries and symmetry violations from high resolution spectroscopy, in: M. Quack, F. Merkt (Eds.), Handbook of High Resolution Spectroscopy, vol. 1, John Wiley & Sons, Ltd, Chichester, New York, 2011, pp. 659–722 (Chapter 18).
[19] M. Quack, On biomolecular homochirality as a quasi-fossil of the evolution of life, in: S.A. Rice, A.R. Dinner (Eds.), Advances in Chemical Physics: Proceedings of the 240 Conference: Science's Great Challenges, vol. 157, Wiley, John Wiley & Sons, Ltd, 2014, pp. 249–290 (Chapter 17).
[20] O.N. Kompanets, A.R. Kukudzhanov, V.S. Letokhov, L.L. Gervits, Opt. Commun. 19 (1976) 414–416.
[21] A. Beil, D. Luckhaus, M. Quack, Ber. Bunsenges. Phys. Chem. 100 (1996) 1853–1875.
[22] A. Beil, D. Luckhaus, M. Quack, J. Stohner, Ber. Bunsenges. Phys. Chem. 101 (1997) 311–328.
[23] M. Quack, W. Kutzelnigg, Ber. Bunsenges. Phys. Chem. 99 (1995) 231–245.
[24] C. Daussy, T. Marrel, A. Amy-Klein, C.T. Nguyen, C.J. Bordé, C. Chardonnet, Rev. Lett. 83 (1999) 1554–1557.
[25] M. Quack, J. Stohner, Phys. Rev. Lett. 84 (2000) 3807–3810.
[26] J.K. Laerdahl, P. Schwerdtfeger, H.M. Quiney, Phys. Rev. Lett. 84 (2000) 3811–3814.
[27] M. Quack, J. Stohner, Z. Phys. Chem. 214 (2000) 675–703.
[28] M. Quack, J. Stohner, J. Chem. Phys. 119 (2003) 11228–11240.
[29] J.H. van't Hoff, Vorlesungen über theoretische und physikalische Chemie, Heft 2. Die chemische Statik, Vieweg, Braunschweig, 1899.
[30] M. Quack, Eur. Rev. 22 (2014) S50–S86.
[31] T.R. Doyle, O. Vogl, J. Am. Chem. Soc. 111 (1989) 8510–8511.
[32] M. Diem, D.F. Burow, J. Chem. Phys. 64 (1976) 5179–5185.
[33] M. Diem, D.F. Burow, J. Phys. Chem. 81 (1977) 476–479.
[34] M. Diem, L.A. Nafie, D.F. Burow, J. Mol. Spectrosc. 71 (1978) 446–457.
[35] C. Marcott, T.R. Faulkner, A. Moscowitz, J. Overend, J. Am. Chem. Soc. 99 (1977) 8169–8175.
[36] P. Prasad, D.F. Burow, J. Am. Chem. Soc. 101 (1979) 806.
[37] J. Costante, L. Hecht, P.L. Polavarapu, A. Collet, L.D. Barron, Angew. Chem. Int. Ed. (Engl.) 36 (1997) 885–887.
[38] Z. Vager, E.P. Kanter, G. Both, P.J. Cooney, A. Faibis, W. Koenig, B.J. Zabransky, D. Zajfman, Phys. Rev. Lett. 57 (1986) 2793–2795.
[39] Z. Vager, R. Naaman, E.P. Kanter, Science 244 (1989) 426–431.
[40] R. Dörner, V. Mergel, O. Jagutzki, L. Spielberger, J. Ullrich, R. Moshammer, H. Schmidt-Böcking, Phys. Rep. 330 (2000) 95–192.
[41] M. Pitzer, M. Kunitski, A.S. Johnson, T. Jahnke, H. Sann, F. Sturm, L.P.H. Schmidt, H. Schmidt-Böcking, R. Dörner, J. Stohner, J. Kiedrowski, M. Reggelin, S. Marquardt, A. Schiesser, R. Berger, M.S. Schöffler, Science 341 (2013) 1096–1100.
[42] P. Herwig, K. Zawatzky, M. Grieser, O. Heber, B. Jordon-Thaden, C. Krantz, O. Novotny, R. Repnow, V. Schurig, D. Schwalm, Z. Vager, A. Wolf, O. Trapp, H. Kreckel, Science 342 (2013) 1084–1086.
[43] M. Pitzer, G. Kastirke, M. Kunitski, T. Jahnke, T. Bauer, C. Goihl, F. Trinter, C. Schober, K. Henrichs, J. Becht, S. Zeller, H. Gassert, M. Waitz, A. Kuhlins, H. Sann, F. Sturm, F. Wiegandt, R. Wallauer, L.P.H. Schmidt, A.S. Johnson, M. Mazenauer, B. Spenger, S. Marquardt, S. Marquardt, H. Schmidt-Böcking, J. Stohner, R. Dörner, M. Schöffler, R. Berger, ChemPhysChem 17 (2016) 2465–2472.
[44] A. Beil, H. Hollenstein, O. Monti, M. Quack, J. Stohner, J. Chem. Phys. 113 (2000) 2701–2718.
[45] F. Hobi, R. Berger, J. Stohner, Molec. Phys. 111 (2013) 2345–2362.
[46] S. Albert, K. Keppler Albert, P. Lerch, M. Quack, Faraday Discuss. 150 (2011) 71–99.
[47] S. Albert, P. Lerch, R. Prentner, M. Quack, Angew. Chem. Int. Ed. (Engl.) 52 (2013) 346–349.
[48] S. Albert, P. Lerch, M. Quack, ChemPhysChem 14 (2013) 3204–3208.
[49] S. Albert, K. Keppler, P. Lerch, M. Quack, A. Wokaun, J. Mol. Spectrosc. 315 (2015) 92–101.
[50] S. Albert, F. Arn, I. Bolotova, Z. Chen, C. Fábri, G. Grassi, P. Lerch, M. Quack, G. Seyfang, A. Wokaun, D. Zindel, J. Phys. Chem. Lett. 7 (2016) 3847–3853.
[51] M. Snels, V. Horká-Zelenková, H. Hollenstein, M. Quack, High resolution FTIR and diode laser spectroscopy of supersonic jets, in: M. Quack, F. Merkt (Eds.), Handbook of High Resolution Spectroscopy, vol. 2, Wiley, John Wiley & Sons, Ltd, 2011, pp. 1021–1067 (Chapter 27).
[52] A. Maki, J.S. Wells, Wavenumber Calibration Tables from Heterodyne Frequency Measurements, NIST Special Publication 821, USA, 1991.
[53] H. Hollenstein, M. Quack, E. Richard, Chem. Phys. Lett. 222 (1994) 176–184.
[54] M. Snels, A. Beil, H. Hollenstein, M. Quack, U. Schmitt, F. D'Amato, J. Chem. Phys. 103 (1995) 8846–8853.
[55] B.P. Winnewisser, J. Reinstädtler, K.M.T. Yamada, J. Behrend, J. Mol. Spectrosc. 136 (1989) 12–16.
[56] W. Quapp, S. Albert, B.P. Winnewisser, M. Winnewisser, J. Mol. Spectrosc. 160 (1993) 540–553.
[57] S. Albert, M. Winnewisser, B.P. Winnewissser, Ber. Bunsenges. Phys. Chem. 100 (1996) 1876–1896.
[58] A. Maki, W. Quapp, S. Klee, G.C. Mellau, S. Albert, J. Mol. Spectrosc. 185 (1997) 356–369.
[59] S. Albert, M. Winnewisser, B.P. Winnewissser, Microchim. Acta 14 (1997) 79–88.
[60] S. Albert, M. Winnewisser, B.P. Winnewissser, Ber. Bunsenges. Phys. Chem. 101 (1997) 1165–1186.
[61] S. Albert, K. Albert, M. Winnewisser, B.P. Winnewissser, Ber. Bunsenges. Phys. Chem. 102 (1998) 1428–1448.
[62] S. Albert, M. Winnewisser, B.P. Winnewissser, J. Mol. Struct. 599 (2001) 347–369.
[63] S. Albert, K. Keppler Albert, H. Hollenstein, C. Manca Tanner, M. Quack, Fundamentals of rotation-vibration spectra, in: M. Quack, F. Merkt (Eds.), Handbook of High-Resolution Spectroscopy, vol. 1, John Wiley & Sons, Ltd, Chichester, 2011, pp. 117–173 (Chapter 3).
[64] S. Albert, M. Quack, J. Mol. Spectrosc. 243 (2007) 280–291.
[65] S. Albert, K.K. Albert, M. Quack, J. Mol. Struct. 695–696 (2004) 385–394.
[66] S. Albert, H. Hollenstein, M. Quack, M. Willeke, Mol. Phys. 102 (2004) 1671–1686.
[67] S. Albert, S. Bauerecker, M. Quack, A. Steinlin, Mol. Phys. 105 (2007) 541–558.
[68] S. Albert, C. Manca Tanner, M. Quack, Mol. Phys. 108 (2010) 2403–2426.
[69] J.K.G. Watson, in: J. Durig (Ed.), Vibrational Spectra and Structure, vol. 6, Elsevier, Amsterdam, 1978, pp. 1–89.
[70] D. Luckhaus, M. Quack, Mol. Phys. 68 (1989) 745–758.
[71] M. Quack, Chem. Phys. Lett. 132 (1986) 147–153.
[72] S.K. Tokunaga, C. Stoeffler, F. Auguste, A. Shelkovnikov, C. Daussy, A. Amy-Klein, C. Chardonnet, B. Darquié, Mol. Phys. 111 (2013) 2363–2373.

[73] E. Hirota, Proc. Jpn. Acad. Ser. B 88 (2012) 120–128.

[74] D. Patterson, M. Schnell, J.M. Doyle, Nature 497 (2013) 475–477.

[75] A. Zehnacker, M. Suhm, Angew. Chem. Int. Ed. (Engl.) 47 (2008) 6970–6992.

[76] N.A. Seifert, C. Perez, J.L. Neill, B.H. Pate, M. Vallejo-Lopez, A. Lesarri, E.J. Cocinero, F. Castano, Phys. Chem. Chem. Phys. 17 (2015) 18282–18287.

[77] E.R. Cohen, T. Cvitas, J.G. Frey, B. Holstrom, K. Kuchitsu, R. Marquardt, I. Mills, F. Pavese, M. Quack, J. Stohner, H.L. Strauss, M. Takami, A.J. Thor. Quantities, Units and Symbols in Physical Chemistry, The Royal Society of Chemistry, 3rd revised printing, 2011.